Multiple binding sites for resin-acid derivatives on the voltage-sensor domain of the Shaker potassium channel

Malin Silverå Ejneby[1], Arina Gromova[2], Nina E Ottosson[1], Stina Borg[2], Argel Estrada-Mondragón[1], Samira Yazdi[2], Panagiotis Apostolakis[2], Fredrik Elinder[1,*] & Lucie Delemotte[2,*]

[1]Department of Biomedical and Clinical Sciences, Linköping University, Linköping, Sweden
[2]Science for Life Laboratory, Department of Applied Physics, KTH Royal Institute of Technology, Stockholm, Sweden

[*]To whom correspondence should be addressed

ABSTRACT
Resin acids and their derivatives open voltage-gated potassium (K_V) channels by attracting the positively charged voltage sensor helix of the channel (S4) towards the extracellular leaflet of the cellular membrane and thereby favoring gate opening. The resin acids have been proposed to primarily bind in a pocket in the periphery of the channel, located between the lipid-facing extracellular ends of the transmembrane segments S3 and S4. However, neutralization of the top gating charge of the Shaker K_V channel unexpectedly increases the resin-acid induced opening, suggesting other mechanisms and possibly other sites of action. Here we explored the binding of two resin-acid derivatives, Wu50 and Wu161, to the Shaker K_V channel by a combination of *in-silico* docking, molecular dynamics simulations, and electrophysiological study of mutated channels. We identified three potential resin-acid binding sites around the voltage sensor helix S4: (1) the S3/S4 site identified in our previous work, (2) a site located in the cleft between S4 and the pore domain (the S4/pore site), and (3) a site located at the extracellular side of the voltage-sensor domain in a cleft formed by S1-S4 (the top-VSD site). The presence of multiple binding sites around S4 and the anticipated helical-screw motion of the helix during activation makes the effect of resin acid derivatives on channel function intricate. The propensity of a specific resin acid to open/close a voltage-gated channel likely depends on its exact binding pose and the types of interactions it can form with the protein in a state-specific manner.

INTRODUCTION

Resin acids, which are primarily found in pine resin, and their chemical derivatives promote the opening of several voltage-gated potassium (K_V) channels (Ottosson et al., 2015, 2017, 2014; Sakamoto et al., 2017; Salari et al., 2018; Silverå Ejneby et al., 2018) and the voltage-gated and calcium-activated BK channel (Imaizumi et al., 2002; Sakamoto et al., 2006). A naturally occurring resin acid has also been shown to promote inactivation of voltage-gated sodium and calcium channels (Salari et al., 2018). One example of resin-acid activated K_V channel is the human M-type K_V channel (hK_V7.2/7.3), which regulates excitability of nerve cells of the brain (Brown and Adams, 1980; Wang et al., 1998) . Resin-acid derivatives are therefore interesting drug candidates for the treatment of hyper-excitability related diseases such as epilepsy (Kobayashi et al., 2008; Ottosson et al., 2015; Silverå Ejneby et al., 2018; Wu et al., 2014a).

In contrast to many other channel-targeting compounds, resin acids and their derivatives are relatively hydrophobic (LogP ≈ 6), because of their three-ringed structure. As such, they have been suggested to partition into the lipid bilayer and interact with the Shaker K_V channel from the membrane-facing side (red triangle in Fig. 1A,B; Ottosson et al., 2017). The negatively charged resin acid is suggested to electrostatically pull the positively charged S4 helix upward, while rotating clockwise when viewed form the extracellular side (Ottosson et al., 2014, 2015, 2017; Silverå Ejneby et al., 2018). In turn, this activation of the voltage sensor promotes gate opening in the pore domain of the channel. The resin acids shift the conductance-versus-voltage, *G(V)*, curve towards more negative membrane voltages and, in most cases, increase the maximum conductance, G_{MAX} (Fig. 1C). The $G(V)$ shift and the G_{MAX} increase can be caused by a common site and mechanism of action. But, at least for polyunsaturated fatty acids, which share some functional properties with the resin acids (Ottosson et al., 2014), it has been suggested that these two effects on the cardiac K_V7.1 channel are mediated via two different parts on the channel (Liin et al., 2018b).

Two experimental findings are supporting the electrostatic channel-opening mechanism: (1) The addition of two positively charged residues at the top of S4 of the *Drosophila* Shaker K_V channel [M356R/A359R (=R_{-1} and R_0 in Fig. 1B), from hereon called the 2R motif] increases the channel-opening effect of resin acids (*G(V)*-shift towards more negative membrane voltages; Ottosson et al., 2014, 2015, 2017; Silverå Ejneby et al., 2018). (2) Substituting the negative charge on the resin acid by a positive one promotes channel closing (*G(V)*-shift towards more positive membrane voltages; Ottosson et al., 2017). Mutagenesis and molecular modeling experiments are consistent with resin-acid derivatives binding between the extracellular portions of S3 and S4, located in the periphery of the voltage-sensor domain (VSD; Fig. 1A,B) (Ottosson et al., 2017).

However, some phenomena cannot easily be explained by this simple mechanism: neutralizing the outermost endogenous gating charge R362 to glutamine (R362Q = R1Q) of the WT Shaker K_V channel has surprising effects on the *G(V)*-shifting effects of some resin-acid derivatives (Ottosson et al., 2017; Silverå Ejneby et al., 2018). Using the simple model

presented above, we would expect that neutralization of R362 to systematically *decrease* the *G(V)*-shifting effect. Instead, the neutralization of R362 led to an *increase* in effect for two resin acids (DHAA and Wu32) and to *no noticeable change* for the more flexible Wu161, and for the polyunsaturated fatty acid docosahexaenoic acid (DHA; a charged lipophilic compound also interacting electrostatically with S4) (Börjesson et al., 2010; Börjesson and Elinder, 2011; Yazdi et al., 2016) (Fig. 1D). Thus, a single binding site, common for all resin-acid derivatives, located at the S3/S4 interface cannot easily explain why the *G(V)* shift increases for some resin acids upon R362Q mutation.

To be able to design and develop more potent and selective compounds it is imperative to understand the molecular action on ion channels in detail. Therefore, in this work, we sought to explore the molecular mechanism of action of resin-acid derivatives binding with respect to the following questions: (1) Why do resin-acid derivatives have a larger *G*(*V*)-shifting effect on the Shaker K_V channel with the 2R motif compared to the WT Shaker K_V channel? (2) Why does the R362Q mutation increase the shift for the compact compounds (e.g. Wu50, Wu32, DHAA) instead of reducing it? (3) Why are more flexible compounds (e.g. Wu161, DHA) less affected by the R362Q mutation than the more compact ones?

We performed docking and molecular dynamics simulations (MD) to identify new possible binding sites in the Shaker K_V channel and characterize the molecular determinants of binding, and site-directed mutagenesis to test these predictions. We conclude that three possible interaction sites are available around S4 of the Shaker K_V channel, making for a complex, state-dependent interaction pattern.

METHOD

Expression of Shaker K_V channels in *Xenopus laevis* oocytes

The Shaker H4 channel (Accession no. NM_167595.3) (Kamb et al., 1987), with removed N-type inactivation due to a Δ6-46 deletion (ShH4IR, in Bluescript II KS[+] plasmid) (Hoshi et al., 1990), is referred to as the WT Shaker K_V channel. Addition of two positively charged arginines (M356R/A359R) at the extracellular top of the voltage sensor increases the effect of charged lipophilic compounds (Ottosson et al., 2014, 2015, 2017). Since the endogenous arginine R362 (=R1) was found to be important for large effect of polyunsaturated fatty acids on the M356R/A359R channel (Ottosson et al., 2014), this channel was referred to as the 3R Shaker K_V channel. However, for the resin-acid derivatives studied in the present investigation, R362 reduced the effect. Therefore, we specifically refer to the two added arginines just outside S4 (M356R/A359R) as the 2R motif. Mutations were introduced with site-directed mutagenesis and verified with sequencing as described previously (Börjesson et al., 2010). RNA injection and oocyte handling were carried out as before (Börjesson et al., 2010; Ottosson et al., 2015). All animal experiments were approved by the Linköping's local Animal Care and Use Committee.

Electrophysiology

Electrophysiological experiments were made 1–6 days after RNA injection. K currents were measured with the two-electrode voltage-clamp technique (GeneClamp 500B amplifier; Axon Instruments) as described previously (Ottosson et al., 2015; Silverå Ejneby et al., 2018). The amplifier's leak compensation was used, and the currents were low-pass filtered at 5 kHz. The control solution contained (in mM): 88 NaCl, 1 KCl, 15 HEPES, 0.4 $CaCl_2$, 0.8 $MgCl_2$ and pH was set with NaOH. All experiments made in room temperature (20–23°C). The holding potential was set to −80 (or –100 mV if the mutant was not fully closed at –80 mV).

Resin-acid derivatives

Synthesis of Wu50 (Ottosson et al., 2015), Wu161, and Wu181 (Silverå Ejneby et al., 2018) and has been described previously. Stock solutions were stored at –20°C, and diluted in control solution just prior to experiments. The test solution was added to the oocyte bath manually with a syringe. Wu161 and Wu181 are permanently negatively charged, while the apparent pK_a in lipid membrane for Wu50 is around 6.5 (Ottosson et al., 2015). To make sure all Wu50 molecules were negatively charged the pH of the control solution was set to 9.0 before the experiments.

Analysis of electrophysiological measurements

The conductance, *G(V)*, was calculated as,

$$G(V) = I / (V - V_K), \quad (1)$$

where I is the steady-state current measured at the end of each test-voltage sweep (100 ms after onset, Clampfit 10.5, Molecular Devices), V the absolute membrane voltage and V_K the reversal potential for K ions (set to –80 mV). The conductance was fitted with a Boltzmann equation (GraphPad Prism 5, GraphPad Software, inc),

$$G_K(V) = G_{MAX} / (1 + \exp((V_{½} - V)/s)^n, \quad (2)$$

where G_{MAX} is the amplitude (maximal conductance) of the curve, V the absolute membrane voltage, $V_{½}$ the midpoint, s the slope, and n an exponent sometimes used for better curve fit. For the estimation of $V_{½}$ and G_{MAX}, n was set to 1. For illustrative purposes n was set to 4. The resin-acid induced *G(V)* shift was calculated as $V_{½}$ (compound) – $V_{½}$ (control). The relative change in G_{MAX} was calculated as G_{MAX} (compound) / G_{MAX} (control). The concentration dependence for the *G(V)* shifts were calculated as,

$$\Delta V = \Delta V_{MAX} / (1 + EC_{50}/c), \quad (3)$$

where ΔV is the voltage shift, ΔV_{MAX} the voltage shift at saturating concentration, c the concentration of the tested compound, and EC_{50} the concentration at which half maximum response occurs.

Molecular docking

A previously published model of the Shaker K_V channel in the activated/open state was used as the receptor in docking experiments (Yazdi et al., 2016). Initial coordinates for bound resin acid derivatives Wu50 and Wu161 were obtained using molecular docking to three different binding sites localized around the outer arginine residues on S4. The docking box was placed around the center of the upper portion of the cleft between S3 and S4 for the S3/S4 site, around the geometric center of the group defined by residues R362, R365, and W454 for the S4/pore site, and around the center of the upper portion of the 4-helix VSD bundle for the top-VSD site. Docking was performed using Autodock Vina (Trott and Olson, 2010). Since the Autodock Vina scoring function does not account for lipid bilayer environment, the ranking of the docking positions is only approximate. We thus selected docking positions based on a few physical principles: the charged headgroup of the resin acid derivatives had to localize in the headgroup region, and in direction of positively charged protein groups, while the hydrophobic body localized in the lipid tail region. The coordinates of the ligands docking pose that were subsequently used as initial conditions for the MD simulations are provided on the Open Science Framework repository (https://osf.io/fw8h9/).

Molecular dynamics (MD) simulations

The MD simulation system, mimicking the ion channel in its environment, was constructed using the CHARMM GUI Membrane Builder (Wu et al., 2014b). The channel and its ligand were placed in a phosphatidylcholine (POPC) bilayer, and the system was hydrated with a 150 mM KCl solution. Mutations (as described in Table 1) were also introduced CHARMM GUI. The Charmm36 force field was used to describe interactions between protein, lipid and ion atoms, the TIP3P model was used to describe the water particles. The ligand was considered in its charged form, and topology and parameters were prepared using the SwissParam software (Zoete et al., 2011). MD simulations were performed using Gromacs version 5.1.2 (Abraham et al., 2015) on the Beskow supercomputer located at PDC, KTH. The simulations were performed in sequential steps of minimization, equilibration and production, keeping the default CHARMM GUI parameters (Lee et al., 2016). Initially, 500 ns of simulations were performed for each system. They were then extended for selected systems (Table 1).

Table 1: Systems simulated and length of trajectories

#	Site	Compound	Mutation	Length [ns]
1	S3/S4	Wu50	WT	1000
2	S3/S4	Wu50	2R	500
3	S4/pore	Wu50	WT	500
4	S4/pore	Wu50	W454A	500
5	S4/pore	Wu50	R362Q	500
6	S4/pore	Wu50	W454A/R362Q	1000
7	S4/pore	Wu50	R362Q/R365Q	1000
8	S4/pore	Wu50	R362Q/R365Q/W454A	640
9	S3/S4	Wu161	WT	500
10	S4/pore	Wu161	WT	500
11	Top-VSD	Wu50	WT	500

MD simulation analysis
Simulation data analysis was performed by scripts using the Python library MDTraj (McGibbon et al., 2015) and are available for download on OSF (https://osf.io/fw8h9/). First, the shortest distance between any heavy atom of the residue in focus and any heavy atom of the ligand were calculated along time. Then the contact frequency was extracted as the fraction of production simulation time spent with any ligand heavy atom within a 4.5 Å cutoff of any residue heavy atom. Data is reported for the four subunits independently, and can be seen as four simulation replicates informing on the replicability of the results. Visualization and figure rendering were performed using Visual Molecular Dynamics (VMD) (Humphrey et al., 1996).

Statistics
Average values are expressed as mean ± SEM. When comparing two resin acid-induced *G(V)* shifts or EC_{50} values, a two-tailed unpaired t-test was used.

RESULTS

The 2R motif increased the maximum *G*(*V*) shift of three resin acid derivatives
In previous work we suggested that resin-acid derivatives open the Shaker K_V channel by binding to the S3/S4 cleft (Fig. 1A,B; Ottosson et al., 2017). One of the arguments supporting this interaction site was that the double-arginine mutation M356R/A359R in the top of S4 (the 2R motif of the Shaker K_V channel) increased the *G*(*V*)-shifting effect of resin acids and polyunsaturated fatty acids substantially (Ottosson et al., 2014). To get information on how the apparent affinity (EC_{50}) and efficacy (maximum *G*(*V*) shift, ΔV_{MAX}) is affected by the double-arginine mutation M356R/A359R we explored the concentration dependence of Wu50 (Fig. 1E) at pH 9.0 (a pH at which the compound is fully charged; Ottosson et al., 2015), and of the permanently charged compounds Wu161 (Fig. 1F) and Wu181 (Fig. 1G; Silverå Ejneby et al., 2018) at pH 7.4. The 2R motif increased the Wu50-induced maximum *G(V)* shift by 57% (from –36.1 ± 1.3 mV, *n* = 3-5, to –56.5 ± 2.6 mV, *n* = 4-10), but with no effect in apparent affinity (EC_{50}(WT) = 29.1 ± 3.5 µM, n = 3-5; EC_{50}(2R) = 30.0 ± 5.0 µM, *n* = 4-10; Fig. 1E). In contrast to the relatively small increase in *G*(*V*) shift for Wu50, the double-arginine mutation increased the maximum *G*(*V*) shift for Wu161 by 230% (from –13.9 ± 0.6 mV, *n* = 3-4, to –45.5 ± 3.5 mV, *n* = 3-6), and for Wu181 by 590% (from –7.8 ± 0.5 mV, *n* = 2-3, to –53.6 ± 4.0 mV, *n* = 4-5). While the apparent affinity was not affected for Wu161 (EC_{50}(WT) = 43.7 ± 6.3 µM, *n* = 3-4; EC_{50}(2R) = 36.4 ± 9.0 µM, *n* = 3-9), it seemed to slightly decrease for Wu181, but this effect was not statistically significant (EC_{50}(WT) = 1.6 ± 0.6 µM, *n* = 2-3; EC_{50}(2R) = 6.1 ± 1.7 µM, *n* = 4-5). In summary, while the maximum *G*(*V*) shift was about equal for all three compounds on the Shaker K_V channel with the 2R motif (–46 to –57 mV), the maximum shift on the WT Shaker K_V channel was much smaller for the two flexible stalk compounds (Wu161 and Wu181; –8 and –14 mV) compared with the more compact Wu50 (–36 mV). The apparent affinity, however, was not dependent on channel mutations, but compound-dependent, with Wu181 being the most potent compound. Because

the oocytes in many experiments did not tolerate higher concentrations of Wu181, we used Wu50 and Wu161 for the remainder of this study.

The 2R motif increased the binding of Wu50 to the S3/S4 cleft

To gain insight at the molecular level about the effect of the double-arginine mutation (M356R/A359R = the 2R motif), we turned to molecular docking and MD simulations. While MD simulations do not assess efficacy, they provide an indication of the kinetics of unbinding from the active state of the Shaker K_V channel through the observation of a few stochastic events. Since the channel considered here is a homotetramer, each simulation provides four quasi-independent observations, and each subunit can be considered as a replicate simulation. Overall, if compounds tend to detach easily from their initial binding pose, this may indicate that there is no free energy minimum at the initial docking pose location. When compounds seem to stay stably bound, this can serve as an indication of a high free energy barrier towards unbinding, and thus indirectly of a putative high binding affinity. In this section we describe docking of Wu50, while Wu161 is explored further down in the text.

Docking of Wu50 to the S3/S4 site of the fully activated/open WT Shaker K_V channel, followed by a 1 μs long simulation of this system, revealed a pose in which the negatively charged carboxyl group of Wu50 was localized in the headgroup region of the lipid bilayer and interacted with polar residues Thr326 or Thr329 (in the extracellular end of S3), or with the positively charged residue Lys266 (in the S1-S2 loop), while its hydrophobic body partitioned in the lipid tail region and was in contact with hydrophobic residues of the S3/S4 upper cleft Ile325, Ala359, Ile360 and Ile364 (Fig. 2A-D). The binding pose, however, appeared quite unstable in three out of four subunits (Fig. 2B). In one of the subunits, the orientation of the compound even changed drastically, assuming a position parallel to the membrane surface, with the negatively charged headgroup reaching out of the pocket towards R362 (Subunit C, Fig. 2A,C). In two subunits (Subunits A and B, Fig. 2A-C), the compound eventually detached from the binding site after a few hundreds of nanoseconds. We noted that this occurred in the two subunits where Lys266 pointed away from the binding site, while in subunit D, where Lys266 pointed towards the binding site, the binding of Wu50 remained stable over the entire length of the MD simulation. We thus conclude that binding to the S3/S4 cleft appeared relatively weak and that the charged residues present at the top of the VSD played a role in keeping Wu50 close to the channel.

To further test the role of positively charged residues on S4, we docked Wu50 to the S3/S4 cleft in the fully activated/open Shaker K_V channel with the 2R motif (Fig. 2E-H). In all subunits, the negative charge of Wu50 quickly oriented towards M356R and/or A359R (Fig. 2G,H). This interaction maintained the hydrophobic body in contact with I360 for more than 80% of the simulation time and with I325 for more than 50% of the simulation time in all subunits (Fig. 2G). While different subunits displayed different behaviors, this site clearly appeared more stable than in the WT channel. The electrostatic potential at the pocket, which is heavily influenced by the presence or absence of positively charged residues, thus seems to control the affinity of the negatively charged compound for the S3/S4 the binding site.

Electrophysiology data (Fig. 1E) indicate that the apparent efficacy of Wu50 towards the Shaker K_V channel with or without the 2R motif differs while its affinity to both channels is similar. The apparent difference in affinity inferred from the MD simulations, as well as the unexplained behavior of the R362Q mutant for some resin acids (Fig. 1D), could be an indication of the presence of other binding sites in the channel's periphery.

A S4/pore pocket is important for Wu50 effects

In the absence of a modulator compound, R362 (and R365) of the active state Shaker K_V channel electrostatically interacts with the PO_4^- group of zwitterionic POPC lipids forming the membrane (Fig. 3A) (Kasimova et al., 2014). This interaction disappears when the channel deactivates, that is as the S4 helix moves down in a helical-screw motion (Tombola et al., 2007). Indeed, during the first steps of deactivation, R362 and R365 leave the lipid headgroups to interact with negatively charged amino acids located on helices S1-S3. It follows therefrom that when the upper leaflet contains negatively charged lipids, the activated state is stabilized through an electrostatic effect, which is reflected through a *G(V)*-shift towards more negative membrane voltages. When lipid headgroups are absent, on the other hand, a *G(V)*-shift towards more positive membrane voltages appears and the activated state can be destabilized due to the lack of binding site for R362 and R365 in the activated state (Kasimova et al., 2014). The environment around the S4 helix seems thus to be able to accommodate compounds that are both hydrophobic and negatively charged when the channel is fully activated.

We thus hypothesized that the S4/pore pocket may harbor a potential stable binding site for a negatively charged compound such as Wu50. To test this hypothesis, we docked Wu50 to the fully activated/open WT Shaker K_V channel, centering the docking box close to the PO_4^- group coordinating R362. The 500 ns MD simulations initiated from this pose indicated that Wu50 tended to stay in this pocket (Fig. 3B,C, S1, S7). The negatively charged carboxyl group of Wu50 made a close interaction with the positively charged R362. In addition, Wu50 displayed a prominent interaction with a tryptophan residue located in the extracellular end of S6 (W454) (Fig 3C, S1). In some subunits, the flat aromatic sidechain ring of W454 formed a tight parallel interaction with the flat tri-chlorinated aromatic skeleton ring of Wu50 (Fig. 3C). A phenylalanine residue located in the extracellular end of S5 (F416) closed the binding site on the other side (Fig. 3C, S1). The stable and simultaneous interaction with R362 and W454 would be lost as the channel deactivates and S4 moves down while R362 rotates away from the S4/S5 cleft. We thus hypothesize that binding to this site, which we call the S4/pore site, stabilizes the VSD activated state and therefore promotes channel opening.

To experimentally test a potential binding site between R362 and W454 we mutated these residues one by one and in combination. As mentioned in the Introduction, removing the top gating charge (R362Q) did not decrease the effect but increased it (Fig. 3E,G, Table S1), from –25.5 ± 1.4 mV (n = 5) to –49.6 ± 1.2 mV (n = 3). In contrast, if the tryptophan 454 in S6 was mutated to an alanine, the *G(V)*-shift was substantially reduced (Fig. 3F,G, Table S1), from –25.5 ± 1.4 mV (n = 5) to –8.1 ± 0.4 mV (n = 5). (There is also a clear reduction in G_{MAX}; this will be dealt with further down in the text). For the W454A mutation we hypothesize that the

reduced $G(V)$ shift is due to reduced binding to this site (between R362 and W454), as indicated by a slight increase in instability of Wu50 binding at this site in MD simulations (Fig. S2, S7). MD shows that Wu50 finds a deeper binding site between F416, R362 and R365 (Fig. 3I). This binding will clearly reduce the channel opening capacity. In contrast, when R362 is neutralized, we think that Wu50 remains bound to W454, but interacts electrostatically with R365, thus favoring activation (Fig. 3I). MD simulations are not able to capture this conformational change since it presumable requires crossing significant free energy barriers associated with further rotation of S4 (Fig. S3, S7). This, at first sight surprising, this finding is consistent with our previous results on two other resin acids (DHAA and Wu32) showing an increased $G(V)$ shift upon mutation of R362 (Ottosson et al., 2017; Silverå Ejneby et al., 2018); illustrated in Fig. 1D.

Surprisingly, simultaneously mutating W454 and R362 (R362Q/W454A) did not significantly reduce the effect (Fig. 3G, –41.0 ± 4.4, n = 5) compared to R362Q. A possible explanation for this phenomenon was found in the MD simulations; in the absence of R362, Wu50 could instead be coordinated by R365, and the aromatic F416 could replace the aromatic W454 (Fig. S4 and 3G, H, I). We hypothesize that the reason for the larger effect on R362Q/W454A (–41.0 mV) than on WT (–25.5 mV) is that the site between R365 and F416 is not accessible when R362 is an arginine. To experimentally test the idea that R365 is important for the effect, we also neutralized R365 (R362Q/R365Q). The $G(V)$ shift was very much reduced from –49.6 ± 1.2 mV (n = 3; R362Q) to –25.5 ± 4.6 mV (n = 5; R362Q/R365Q) (Fig. 3G), thus supporting the hypothesis of a site between R365 and F416. In line with this, the R362Q/R365Q/W454A mutation showed the same sensitivity to Wu50 (–24.7 ± 3.0, n = 6; Fig. 3G, Table S1). We tried to explore the role of F416 by mutating it to an alanine (R362Q/W454A/F416A). However, Wu50 almost completely blocked this channel (83 ± 6% reduction, n = 5; Table S1, Fig. 3J) making it problematic to evaluate any shift in $G(V)$.

Alterations in the S4/pore pocket turn Wu50 into a conductance-reducer

As mentioned in the introduction, many channel-opening compounds, including the resin-acid derivatives, both shift the $G(V)$ in negative direction along the voltage axis *and* increase the G_{MAX}. While we do not know the mechanism for this G_{MAX} increase, the shift and the increase are in many cases connected – a compound with large $G(V)$-shifting effect also has a large increase in G_{MAX}, and some mutations increasing the $G(V)$ shift also increase G_{MAX}. However, in the present study we found several channels with mutations in the S4/pore pocket where Wu50 instead acts as a G_{MAX} reducer (Fig. 3F, J, Table S1). The W454A mutation caused a clear Wu50-induced G_{MAX} reduction (G_{MAX} = 0.56 ± 0.08, n = 5). It is likely that Wu50 binds between R362 and F416 to produce a very diminished $G(V)$ shift and to reduce the G_{MAX}. F416 has been suggested to play a critical role for communication between the VSD and the pore domain to regulate slow (C-type) inactivation of the channel (Conti et al., 2016). Possibly pulling in F416 reduces the channel's open probability. In contrast, if R362 is neutralized in addition to W454A, (R362Q/W454A), Wu50 does not reduce G_{MAX} (Fig. 3J; Table S1). Wu50 is probably bound deeper, between R365 and F416, and does not hamper channel opening. Further, by dearomatizing 416 in this channel (R362Q/W454A/F416A) makes Wu50 a strong G_{MAX} reducer (Fig. 3J; Table S1).

In addition, all explored mutations which also contain the R362Q/R365Q mutations turned Wu50 into a current reducer (Fig. 3J, Table S1). The reason is not clear, but one possibility is that Wu50 is bound in a way that affects residue 416 of the pore domain to reduce G_{MAX}. An alternative possibility is that Wu50 also binds to another site that, in the absence of other channel-opening forces reduce G_{MAX} in W454A, R362Q/R365Q, and R362Q/R365Q/W454A. That another site is exposed is also supported by the fact that removal of the aromatic residue in position 454 (W454A) in combination with the R362Q/R365Q mutation does not abolish the $G(V)$ shift (–24.7 ± 3.0, n = 5; Fig. 3G).

The 2R motif rescues the W454A effect and adds to the R362Q effect

When the 2R motif was combined with the *G(V)*-shift-attenuating mutation W454A, the attenuation was gone (Fig. 4A, Table S1), suggesting that the 2R motif trumps the effects of a compound bound to the S4/pore pocket between R362 and W454A. Interestingly, combining the 2R motif with the R362Q mutation increased the $G(V)$ shift even more (from –40.0 ± 2.7 mV, n = 8, to –54.0 ± 2.3 mV, n = 4; Fig. 4B, Table S1). Mutating W454A on this background further had no effect (–56.6 ± 5.8, n = 4; Fig. 4C, Table S1). Thus, we hypothesize that in a channel with the 2R motif, the S3/S4 site dominates and the S4/pore pocket has no additional effect. However, in the absence of R362 (and 2R motif), the binding of the compound in the S4/pore pocket increases the *G(V)* shift through the recruitment of R365, which has a tendency to pull S4 further upwards, and cause opening of the pore at lower potentials.

A longer and more flexible stalk alters Wu161 binding to the S4/pore site

Wu161 and Wu181, which have their negative charge on a three-atom long and slightly flexible stalk, have smaller effects on the WT Shaker K_V channel compared with Wu50, but a very large effect when the 2R motif is introduced (Fig. 1F-G). This suggests that the stalk compounds Wu161 and Wu181 exert their main effect on the Shaker K_V channel with the 2R motif from to the S3/S4 site.

MD simulations initiated with Wu161 docked to the S3/S4 site of the fully activated/open WT Shaker K_V channel did not display a prominently different behavior from Wu50, with two out of four compounds displaying a tendency to leave their binding site (Fig. 5A,B). On the other hand, docking of Wu161 to the S4/pore site showed substantial differences from Wu50 (Fig. 5C,D). The binding to the WT channel appeared overall less stable: Wu161 left the binding site in one of the subunits and the minimum distance from the compound to R362 appeared generally larger and displayed more fluctuations than when with Wu50.

Mutating W454A reduced the *G(V)* shift for Wu161 (from –9.8 ± 1.1 mV, n = 5, to –5.6 ± 0.8 mV, n = 4; Fig. 5E-F; Table S1), suggesting that Wu161 does bind to the S4/pore site, but its effect on the WT Shaker K_V channel is smaller than that of Wu50 (–25.5 ± 1.4; n = 5), which may indicate that binding of this compound to this site is less favorable than that of Wu50, in line with the MD simulation results. Removing R362 does not increase the *G(V)* shift (–8.5 ± 0.5, n = 3), as it does for Wu50 (–49.6 ± 1.2, n = 3; Fig. 5G, Table S1). This may indicate that

while Wu50 fits well between R365 and F416 in the absence of R362 and causes channel opening, Wu161 either does not bind here, or when bound, cannot keep the channel in the open state. In an attempt to further weaken a possible binding of Wu161 to the S4/pore site we tested the triple mutation R362Q/F416A/W454A. The shift was completely eliminated (Table S1) but surprisingly, the compound induced a clear inactivation (Fig. 5H) and the current was clearly reduced (Table S1). We interpret this as if the compound still can bind to the site but not in a way to open the channel but to induce an inactivation, probably by affecting residue 416.

The R362Q/R365Q double mutant reduced the Wu161-induced *G(V)* shift compared with R362Q (from –8.5 ± 0.5, n = 3, to –5.2 ± 1.2, *n* = 4; Fig. 5G, Table S1). Such a reduced effect may indicate that this double mutation abolishes binding of this compound entirely to the S4/pore site. To conclude, the flexible compound Wu161 seems to bind to the S4/pore site, but the binding is less stable than for the more rigid compound Wu50, and the *G*(*V*) shifting effects are substantially smaller (Fig. 5G, blue symbols). In contrast, Wu161 bound to the channel with the 2R motif has a large *G*(*V*) shifting effect (–32.0 ± 2.7 mV, n = 6), indicating stable binding to the S3/S4 site (Fig. 5G, red symbol; Table S1).

A possible binding site at the top of the VSD bundle

Wu50 maintains a substantial shift in the R362Q/R365Q (–25.5 ± 4.6 mV; *n* = 5) and R362Q/R365Q/W454A (–24.7 ± 3.0 mV; *n* = 5) mutants, in the absence of the 2R motif (Fig. 3G), where both the S3/S4 site and the S4/pore site are assumed to be disrupted. This led us to hypothesize that this compound might be able to bind to yet another site in the vicinity of the S4 voltage sensor. Binding to this third site (other than the S3/S4 and S4/pore sites) might shift *G*(*V*). Scrutinizing further the surroundings of S4, we considered a third putative binding pocket in the center of the extracellular domain of the VSD (which we call the top-VSD site, Fig. 6). Indeed, positive charges from S4 (R365, R368, and even R371=R4) are exposed to the extracellular solution, and this site has been shown to be druggable for other classes of compound (Liin et al., 2018a), and in related channels (Ahuja et al., 2015; Li et al., 2013; Peretz et al., 2010).

We thus docked Wu50 to this putative site surrounded by the S1, S2, S3, and S4 helices. Bound here, the negative charge of Wu50 is close to R365 and R368. Other residues often in contact with the compound include F280 and E283 in S2, and T326 in S3 (Fig. 6A-C). Because the negative charge in position 283 (E283, on S2) plays such an important role for gating *per se*, (Papazian et al., 1995) we focused on residues F280 and T326. We first tried R362Q/R365Q/W454A/F280I to explore if dearomatizing F280 was enough to disrupt binding to the top-VSD site (Table S1). However, pH 9, which was routinely used to keep Wu50 fully negatively charged, completely blocked the current, thus preventing exploration of the effect of Wu50. pH 8 only blocked the current by 50 ± 7% (*n* = 4) and allowed us to study the effect of (a possibly not fully-charged) Wu50. Surprisingly Wu50 blocked the channel by 95 ± 2% (n = 4). We speculate that Wu50 still binds in the pocket but that the orientation is altered. Then we tried to explore the effect of Wu50 on R362Q/R365Q/T326C. Again, pH 9 *per se* completely blocked the channel, abrogating the possibility to study the

effect of Wu50. In summary, even though we, for experimental reasons, did not succeed to demonstrate a reduction of the $G(V)$ shift by mutating residues in the putative top-VSD site, both molecular docking and mutational effects do support a putative top-VSD site.

DISCUSSION

The helical-screw motion of S4 combined with the periodic arrangement of arginines every helical turn defines three potential binding sites for resin acids and their derivatives, that can be more or less occupied depending on state- and compound-dependent available interaction motifs (Fig. 7).

Three tentative binding sites

Binding of resin acid compounds to the S3/S4 site (Fig. 7, red triangle) tends to favor S4 activation (Figure 7, displacement towards the right panel) through an electrostatic effect that favors a clockwise motion of S4 when viewed from the top. This site is particularly occupied when the 2R motif is introduced, as evidenced by MD simulations. Binding to this site in the absence of this motif has a relatively minor effect since in the activated state R362 and R365 are located on the opposite side of the S4 helix and R368 and R371 are located too far down. Binding to the S4/pore site (Fig. 7, purple triangle) tends to favor S4 activation through direct binding to R362. The aromatic ring-like body of the resin-acid derivative anchors to W454, or, in its absence, to F416. Removing R362 can enhance the effect of binding to this site since electrostatic pull applies to R365, a residue that is usually buried further into the S4/S5 crevice. The 2R motif, when present, is generally pulled counterclockwise, in a manner that opposes activation. However, the presence of the resin acid at the S3/S4 site has an opposite effect by pulling S4 clockwise and favoring activation. The net effect of binding to these two sites in the presence of the 2R motif appears to favor activation. Finally binding to the top-VSD site has complex effects (Fig. 7, yellow triangle), with R368 and R371 being presumably pulled in a clockwise and upward direction in the activated state, and R362 and R365 being presumably pulled in a counterclockwise and downward direction in the activated state.

The S3/S4 site

Both experimental data and MD simulations have previously been used to describe an interaction site for resin acids in the cleft between S3 and S4 (Fig 7, red) (Ottosson et al., 2017). We have also described that the 2R motif (M356R/A359R) (Fig 7, the top blue residue and the two white residues) greatly enhances the efficacy of resin acids (Ottosson et al., 2014, 2015, 2017; Silverå Ejneby et al., 2018). Here, we have shown that the 2R motif increases the Wu50-induced $G(V)$ shift by 4-32 mV in negative direction along the voltage axis, the size depending on the background mutations. Binding to the S3/S4 site appears to be sensitive to the presence of charges at the extracellular end of S3 and S4. Some channels, such as Kv2.1, have a native arginine at R0 (Fig. S8). For Nav and Cav channels (which are modulated by the resin acid isopimaric acid; Salari et al., 2018), the charge profile varies from subunit to subunit. By designing resin-acid derivatives that primarily bind to the S3/S4 site, as appears to be the case for Wu161 and Wu181, it might be possible to engineer selectivity for specific

channels or specific domains in heteromeric channels. As an example, resin-acid derivatives with a flexible stalk are effective openers of the Shaker K_V channel with the 2R motif ((Silverå Ejneby et al., 2018); present paper) and the Kv7.2/7.3 channel (Silverå Ejneby et al., 2018). Thus, modifications of the stalk can be envisioned to obtain compounds selective for different K_V channel types.

The S4/pore site

In the absence of the 2R motif, the S4/pore site, located between the VSD and the pore (Fig 7, purple), was found to be occupied by resin-acid derivatives. This site could be disrupted by mutating W454A and/or by removing both R362 and R365 (Fig. 3). Binding to the S4/pore site seems to rely on the presence of aromatic residues (W454 and/or F416 in Shaker). A tryptophan in position 454 is unique for the Shaker K_V channel among all K_V channels (Fig. S8), but K_V3 and K_V7 channels have a tryptophan in the neighbor position. F416, on the other hand, is either a phenylalanine or a tyrosine in most K_V channels and could potentially contribute to binding of resin-acid derivatives. Considering the presence of aromatic residues in various channels may be a way to engineer specificity for various channels (Fig. S8).

A promiscuous top-VSD site

Removing the 2R motif and disrupting the S4/pore site was however not enough to render the channel completely insensitive to Wu50. This residual *G(V)* shift could possibly depend on Wu50 binding to another site. Here, we have suggested that Wu50 can bind in a fairly promiscuous drug pocket located in a cleft in the top of the VSD in different voltage-gated ion channels (Fig. 7, yellow; Ahuja et al., 2015; Li et al., 2013; Liin et al., 2018a; Peretz et al., 2010). From here the negatively charged Wu50 could contribute to the negative *G(V)* shift by electrostatically attracting S4 charges to rotate S4 in the clockwise direction, similar to the other sites.

Advantage and challenges of multi-site drug action

Traditional structure-based drug design aims to optimize compounds that fit in and strongly bind to a well-defined pocket of a biomolecule. This work, together with recent developments (Heusser et al., 2018) show that membrane proteins may be druggable via binding of compounds in a state-dependent manner, in different binding sites with similar binding affinity, and via mechanisms involving the membrane (Ahuja et al., 2015; Lambert et al., 2003; Wang, 2011). The resin-acid derivatives studied in this work seem to possess all of these three properties. They seem to differentially stabilize the activated/open and the intermediate/closed state of the Shaker K_V channel depending on their binding to one or more of these three sites. Two of these sites are membrane facing, and binding of the compound to these sites involves displacing a readily bound lipid. While the lipid bilayer has so far often been considered an inert scaffold for membrane proteins, it is now recognized to often play an integral part in modulating protein function and in regulating the access of drug to proteins through competition with the compounds. This indicates that the membrane composition, known to vary from one cell type to the next, also offers possibilities for designing selective drugs with reduced off-target effects. For this to become a rational process, much of the molecular details underlying drug binding remain to be understood and we propose that

studying the effects of resin-acid derivatives on a model channel constitute a first step in this direction.

ACKNOWLEDGEMENT

We thank Xiongyu Wu for synthesis of the compounds Wu50, Wu161, and Wu181 used in this study. We thank Antonios Pantazis for comments on the manuscript. This work was supported by grants from the Swedish Research Council, the Gustafsson Foundation and Science for Life Laboratory to LD, and the Swedish Research Council, the Swedish Brain Foundation, and the Swedish Heart-Lung Foundation to FE. The simulations were performed on resources provided by the Swedish National Infrastructure for Computing (SNIC) at PDC Centre for High Performance Computing (PDC-HPC).

REFERENCES

Abraham, M.J., T. Murtola, R. Schulz, S. Páll, J.C. Smith, B. Hess, and E. Lindahl. 2015. GROMACS: High performance molecular simulations through multi-level parallelism from laptops to supercomputers. *SoftwareX*. 1–2:19–25. doi:10.1016/j.softx.2015.06.001.

Ahuja, S., S. Mukund, L. Deng, K. Khakh, E. Chang, H. Ho, S. Shriver, C. Young, S. Lin, J.P. Johnson, P. Wu, J. Li, M. Coons, C. Tam, B. Brillantes, H. Sampang, K. Mortara, K.K. Bowman, K.R. Clark, A. Estevez, Z. Xie, H. Verschoof, M. Grimwood, C. Dehnhardt, J.-C. Andrez, T. Focken, D.P. Sutherlin, B.S. Safina, M.A. Starovasnik, D.F. Ortwine, Y. Franke, C.J. Cohen, D.H. Hackos, C.M. Koth, and J. Payandeh. 2015. Structural basis of Nav1.7 inhibition by an isoform-selective small-molecule antagonist. *Science*. 350:aac5464. doi:10.1126/science.aac5464.

Börjesson, S.I., and F. Elinder. 2011. An electrostatic potassium channel opener targeting the final voltage sensor transition. *J Gen Physiol*. 137:563–577. doi:10.1085/jgp.201110599.

Börjesson, S.I., T. Parkkari, S. Hammarström, and F. Elinder. 2010. Electrostatic Tuning of Cellular Excitability. *Biophys J*. 98:396–403. doi:10.1016/j.bpj.2009.10.026.

Brown, D.A., and P.R. Adams. 1980. Muscarinic suppression of a novel voltage-sensitive K+ current in a vertebrate neurone. *Nature*. 283:673–676.

Conti, L., J. Renhorn, A. Gabrielsson, F. Turesson, S.I. Liin, E. Lindahl, and F. Elinder. 2016. Reciprocal voltage sensor-to-pore coupling leads to potassium channel C-type inactivation. *Sci Rep*. 6:27562. doi:10.1038/srep27562.

Heusser, S.A., M. Lycksell, X. Wang, S.E. McComas, R.J. Howard, and E. Lindahl. 2018. Allosteric potentiation of a ligand-gated ion channel is mediated by access to a deep membrane-facing cavity. *PNAS*. 115:10672–10677. doi:10.1073/pnas.1809650115.

Hoshi, T., W.N. Zagotta, and R.W. Aldrich. 1990. Biophysical and molecular mechanisms of Shaker potassium channel inactivation. *Science*. 250:533–538.

Humphrey, W., A. Dalke, and K. Schulten. 1996. VMD: Visual molecular dynamics. *Journal of Molecular Graphics*. 14:33–38. doi:10.1016/0263-7855(96)00018-5.

Imaizumi, Y., K. Sakamoto, A. Yamada, A. Hotta, S. Ohya, K. Muraki, M. Uchiyama, and T. Ohwada. 2002. Molecular Basis of Pimarane Compounds as Novel Activators of Large-Conductance Ca2+-Activated K+ Channel α-Subunit. *Mol Pharmacol*. 62:836–846. doi:10.1124/mol.62.4.836.

Kamb, A., L.E. Iverson, and M.A. Tanouye. 1987. Molecular characterization of Shaker, a Drosophila gene that encodes a potassium channel. *Cell*. 50:405–413.

Kasimova, M.A., M. Tarek, A.K. Shaytan, K.V. Shaitan, and L. Delemotte. 2014. Voltage-gated ion channel modulation by lipids: Insights from molecular dynamics simulations. *Biochimica et Biophysica Acta (BBA) - Biomembranes*. 1838:1322–1331. doi:10.1016/j.bbamem.2014.01.024.

Kobayashi, K., Y. Nishizawa, K. Sawada, H. Ogura, and M. Miyabe. 2008. K(+)-channel openers suppress epileptiform activities induced by 4-aminopyridine in cultured rat hippocampal neurons. *J. Pharmacol. Sci.* 108:517–528.

Lambert, J.J., D. Belelli, D.R. Peden, A.W. Vardy, and J.A. Peters. 2003. Neurosteroid modulation of GABAA receptors. *Prog. Neurobiol.* 71:67–80. doi:10.1016/j.pneurobio.2003.09.001.

Lee, J., X. Cheng, J.M. Swails, M.S. Yeom, P.K. Eastman, J.A. Lemkul, S. Wei, J. Buckner, J.C. Jeong, Y. Qi, S. Jo, V.S. Pande, D.A. Case, C.L. Brooks, A.D. MacKerell, J.B. Klauda, and W. Im. 2016. CHARMM-GUI Input Generator for NAMD, GROMACS, AMBER, OpenMM, and CHARMM/OpenMM Simulations Using the CHARMM36 Additive Force Field. *J. Chem. Theory Comput.* 12:405–413. doi:10.1021/acs.jctc.5b00935.

Li, P., Z. Chen, H. Xu, H. Sun, H. Li, H. Liu, H. Yang, Z. Gao, H. Jiang, and M. Li. 2013. The gating charge pathway of an epilepsy-associated potassium channel accommodates chemical ligands. *Cell Res.* 23:1106–1118. doi:10.1038/cr.2013.82.

Liin, S.I., P.-E. Lund, J.E. Larsson, J. Brask, B. Wallner, and F. Elinder. 2018a. Biaryl sulfonamide motifs up- or down-regulate ion channel activity by activating voltage sensors. *J. Gen. Physiol.* 150:1215–1230. doi:10.1085/jgp.201711942.

Liin, S.I., S. Yazdi, R. Ramentol, R. Barro-Soria, and H.P. Larsson. 2018b. Mechanisms Underlying the Dual Effect of Polyunsaturated Fatty Acid Analogs on Kv7.1. *Cell Rep*. 24:2908–2918. doi:10.1016/j.celrep.2018.08.031.

McGibbon, R.T., K.A. Beauchamp, M.P. Harrigan, C. Klein, J.M. Swails, C.X. Hernández, C.R. Schwantes, L.-P. Wang, T.J. Lane, and V.S. Pande. 2015. MDTraj: A Modern Open Library for the Analysis of Molecular Dynamics Trajectories. *Biophys J*. 109:1528–1532. doi:10.1016/j.bpj.2015.08.015.

Ottosson, N.E., S.I. Liin, and F. Elinder. 2014. Drug-induced ion channel opening tuned by the voltage sensor charge profile. *J Gen Physiol*. 143:173–182. doi:10.1085/jgp.201311087.

Ottosson, N.E., M. Silverå Ejneby, X. Wu, S. Yazdi, P. Konradsson, E. Lindahl, and F. Elinder. 2017. A drug pocket at the lipid bilayer-potassium channel interface. *Sci Adv*. 3:e1701099. doi:10.1126/sciadv.1701099.

Ottosson, N.E., X. Wu, A. Nolting, U. Karlsson, P.-E. Lund, K. Ruda, S. Svensson, P. Konradsson, and F. Elinder. 2015. Resin-acid derivatives as potent electrostatic openers of voltage-gated K channels and suppressors of neuronal excitability. *Sci Rep*. 5:13278. doi:10.1038/srep13278.

Papazian, D.M., X.M. Shao, S.A. Seoh, A.F. Mock, Y. Huang, and D.H. Wainstock. 1995. Electrostatic interactions of S4 voltage sensor in Shaker K+ channel. *Neuron*. 14:1293–1301.

Peretz, A., L. Pell, Y. Gofman, Y. Haitin, L. Shamgar, E. Patrich, P. Kornilov, O. Gourgy-Hacohen, N. Ben-Tal, and B. Attali. 2010. Targeting the voltage sensor of Kv7.2 voltage-gated K+ channels with a new gating-modifier. *Proc. Natl. Acad. Sci. U.S.A.* 107:15637–15642. doi:10.1073/pnas.0911294107.

Sakamoto, K., T. Nonomura, S. Ohya, K. Muraki, T. Ohwada, and Y. Imaizumi. 2006. Molecular Mechanisms for Large Conductance Ca2+-Activated K+ Channel Activation by a Novel Opener, 12,14-Dichlorodehydroabietic Acid. *J Pharmacol Exp Ther*. 316:144–153. doi:10.1124/jpet.105.093856.

Sakamoto, K., Y. Suzuki, H. Yamamura, S. Ohya, K. Muraki, and Y. Imaizumi. 2017. Molecular mechanisms underlying pimaric acid-induced modulation of voltage-gated K+ channels. *Journal of Pharmacological Sciences*. 133:223–231. doi:10.1016/j.jphs.2017.02.013.

Salari, S., M. Silverå Ejneby, J. Brask, and F. Elinder. 2018. Isopimaric acid - a multi-targeting ion channel modulator reducing excitability and arrhythmicity in a spontaneously beating mouse atrial cell line. *Acta Physiol (Oxf)*. 222. doi:10.1111/apha.12895.

Silverå Ejneby, M., X. Wu, N.E. Ottosson, E.P. Münger, I. Lundström, P. Konradsson, and F. Elinder. 2018. Atom-by-atom tuning of the electrostatic potassium-channel modulator dehydroabietic acid. *J. Gen. Physiol.* 150:731–750. doi:10.1085/jgp.201711965.

Tombola, F., M.M. Pathak, P. Gorostiza, and E.Y. Isacoff. 2007. The twisted ion-permeation pathway of a resting voltage-sensing domain. *Nature.* 445:546-549. doi: 10.1038/nature05396.

Trott, O., and A.J. Olson. 2010. AutoDock Vina: improving the speed and accuracy of docking with a new scoring function, efficient optimization and multithreading. *J Comput Chem*. 31:455–461. doi:10.1002/jcc.21334.

Wang, H.-S., Z. Pan, W. Shi, B.S. Brown, R.S. Wymore, I.S. Cohen, J.E. Dixon, and D. McKinnon. 1998. KCNQ2 and KCNQ3 Potassium Channel Subunits: Molecular Correlates of the M-Channel. *Science*. 282:1890–1893. doi:10.1126/science.282.5395.1890.

Wang, M. 2011. Neurosteroids and GABA-A Receptor Function. *Front Endocrinol (Lausanne)*. 2:44. doi:10.3389/fendo.2011.00044.

Wu, C., K. V Gopal, T.J. Lukas, G.W. Gross, and E.J. Moore. 2014a. Pharmacodynamics of potassium channel openers in cultured neuronal networks. *Eur. J. Pharmacol.* 732:68–75. doi:10.1016/j.ejphar.2014.03.017.

Wu, E.L., X. Cheng, S. Jo, H. Rui, K.C. Song, E.M. Dávila-Contreras, Y. Qi, J. Lee, V. Monje-Galvan, R.M. Venable, J.B. Klauda, and W. Im. 2014b. CHARMM-GUI Membrane Builder Toward Realistic Biological Membrane Simulations. *J Comput Chem*. 35:1997–2004. doi:10.1002/jcc.23702.

Yazdi, S., M. Stein, F. Elinder, M. Andersson, and E. Lindahl. 2016. The Molecular Basis of Polyunsaturated Fatty Acid Interactions with the Shaker Voltage-Gated Potassium Channel. *PLoS Comput. Biol.* 12:e1004704. doi:10.1371/journal.pcbi.1004704.

Zoete, V., M.A. Cuendet, A. Grosdidier, and O. Michielin. 2011. SwissParam: A fast force field generation tool for small organic molecules. *Journal of Computational Chemistry*. 32:2359–2368. doi:10.1002/jcc.21816.

FIGURES

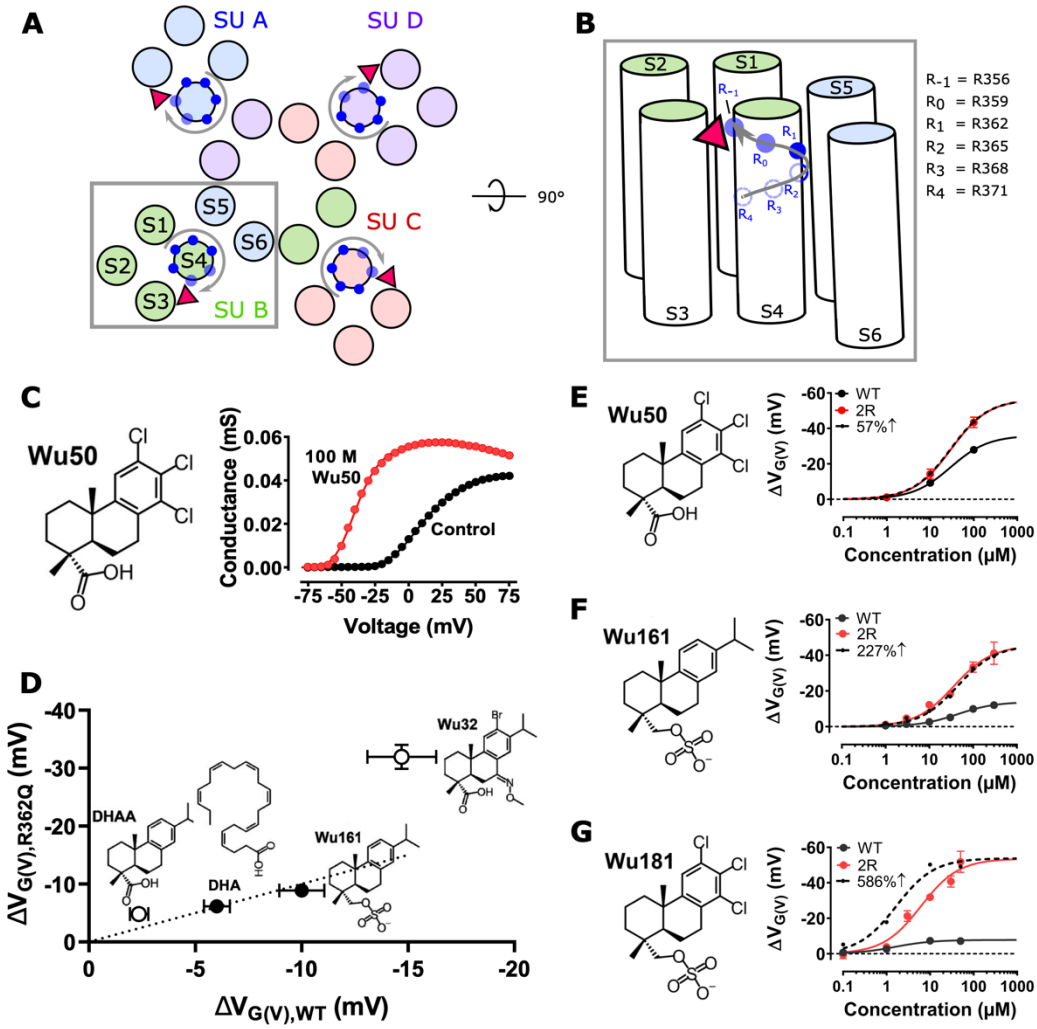

FIGURE 1. The role of S4 mutations in the Shaker K_V channel for the effect of some resin-acid derivatives. A) Top and **B)** side view of the S4 helical-screw motion during voltage-sensor domain activation. The endogenous gating charge arginines (R362 (=R1), R365 (=R2), R368 (=R3), and R371 (=R4)) are denoted by blue filled circles. Additional charges in the 2R motif (M356R, A359R) are denoted by transparent blue filled circles. Binding of a negatively charged compound (red triangle) in the cleft between S3 and S4 (called the S3/S4 site) is hypothesized to favor S4 activation through an electrostatic effect. The homotetrameric channel assembly is shown in A, with each subunit represented in different colors. A single subunit is shown in B (the pore domain and the VSD are from two different subunits). **C)** 100 μM Wu50, at pH 9.0, shifted the $G(V)$ of the Shaker K_V channel with the 2R motif by –40.7 mV. **D)** $G(V)$ shifts for R362Q vs. WT Shaker K_V channels for four compounds. Black symbols represent compound for which the shift is similar in the WT and in the R362Q mutant, while empty symbols represent compounds for which the shift is larger in the mutant. The dotted line has a slope of 1. **E-G)** Concentration-response curves (Eq. 3). Black large symbols and lines are WT Shaker K_V, red symbols and lines are Shaker

K_V with the 2R motif, and black small symbols and dotted lines are WT data scaled to the size of data for the 2R motif. **E)** Wu50, pH = 9.0. WT: EC_{50} = 29.1 ± 3.5 µM, n = 3-5, ΔV_{MAX} = –36.1 ± 1.3 mV, n = 3-5. 2R motif: EC_{50} = 30.0 ± 5.0 µM, n = 4-10, ΔV_{MAX} = –56.5 ± 2.6 mV, n = 4-10. **F)** Wu161, pH = 7.4. WT: EC_{50} = 43.7 ± 6.3 µM, n = 3-4, ΔV_{MAX} = –13.9 ± 0.6 mV, n = 3-4. 2R motif: EC_{50} = 36.4 ± 9.0 µM, n = 3-9, ΔV_{MAX} = –45.5 ± 3.5 mV, n = 3-6. **G)** Wu181, pH = 7.4. WT: EC_{50}(WT) = 1.6 ± 0.6 µM, n = 2-3, ΔV_{MAX} = –7.8 ± 0.5 mV, n = 2-3. 2R motif: EC_{50}(2R motif) = 6.1 ± 1.7 µM, n = 4-5. ΔV_{MAX} = –53.6 ± 4.0 mV, n = 4-5. All data Mean ± SEM.

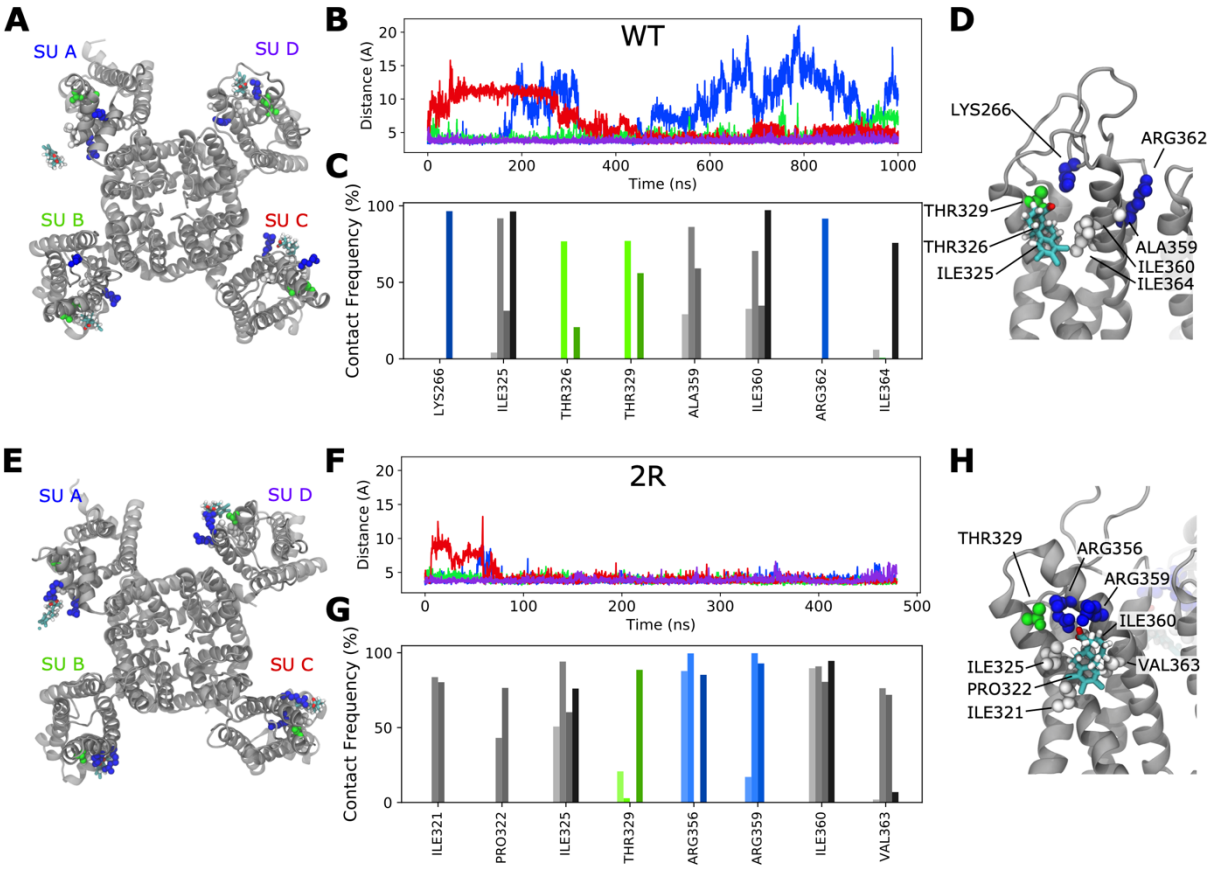

FIGURE 2. Molecular insight into binding of Wu50 to the S3/S4 site A) Top view of a representative snapshot of the interaction between Wu50 and the S3/S4 site in the WT channel. The channel is shown as grey ribbons, the Wu50 compounds are displayed as sticks, each atom type colored differently (cyan: C or Cl; red: O; blue: N and white: H) Apolar, polar and positively charged residues coming in contact with Wu50 in at least one of the channel's subunits are represented as space-filling and depicted in white, green and blue, respectively. **B)** Distance between closest atoms of Wu50 and ILE360 along a 1 µs long MD simulation of the WT channel. Each of four subunits is depicted in a different color, following the color scheme presented in A. **C)** Contact frequency between any atom of Wu50 and S3/S4 site residues in the WT channel MD simulation. Apolar, polar and positively charged residues are depicted in shades of grey, green and blue, respectively. For each residue, each bar corresponds to the contact frequency in one of the four subunits. **D)** Zoomed-in side view of

the S3/S4 site for the WT channel. The residues identified in the contact frequency analysis are shown as space-filling (apolar, polar and positively charged residues depicted in white, green and blue, respectively). Wu50 is displayed as sticks, each atom type colored differently (cyan: C or Cl; red: O; blue: N and white: H) **E)** Top view of a representative snapshot of the interaction between Wu50 and the S3/S4 site in the channel with the 2R motif. **F)** Distance between closest atoms of Wu50 and ILE360 along a 500 ns long MD simulation of the 2R motif-channel system. **G)** Contact frequency between any atom of Wu50 and site 1 residues in the 2R motif channel simulation. **H)** Zoomed-in side view of the S3/S4 site for the channel with the 2R motif. Colors and representations in E-H are the same as in A-D.

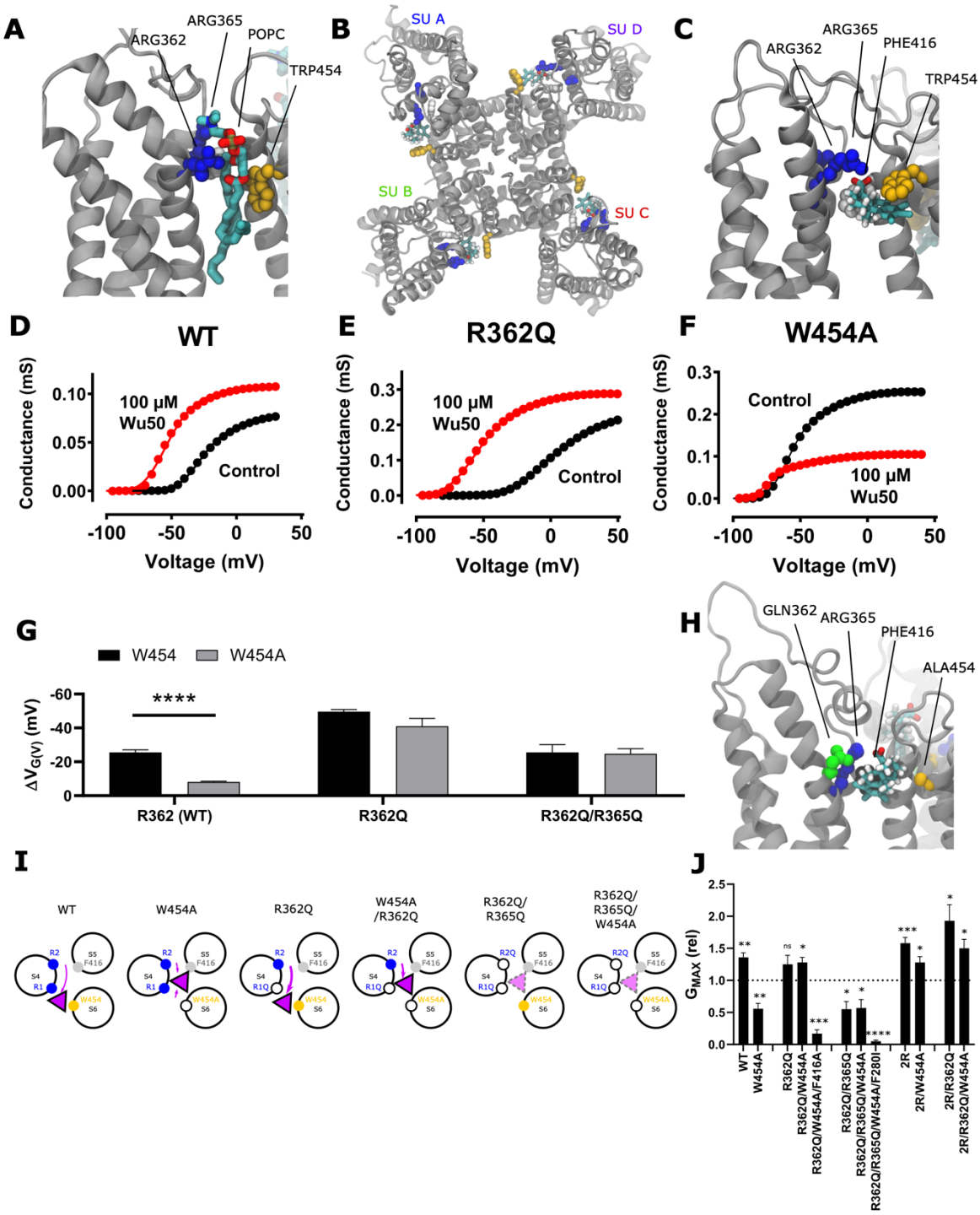

FIGURE 3. A site located at the S4/pore interface is important for the effect of Wu50 on the WT Shaker K_V channel A) Side view of the S4/pore site for the WT channel in the absence of resin acid derivative. A POPC molecule is occupying the binding pocket. POPC is displayed as sticks, each atom type colored differently (cyan: C; red: O; blue: N; brown: P; hydrogens are omitted for clarity). **B)** Top view of a representative snapshot of the interaction between Wu50 and the S4/pore site in the WT channel. the Wu50 compounds are displayed as sticks, each atom type colored differently (cyan: C or Cl; red: O; blue: N and white: H) **C)** Zoomed-in side view of the S4/pore site for the WT channel in the presence of the resin acid

derivative Wu50. **D-F)** Representative $G(V)$ curves for Wu50-induced effects on different Shaker K_V-channel mutants. 100 µM, pH = 9. **G)** Wu50-induced $G(V)$ shifts for different Shaker K_V-channel mutants. 100 µM, pH = 9. Mean ± SEM (n = 3–6). **** = p < 0.0001. **H)** Zoomed-in side view of the modified S4/pore site (site 2') for the W454A/R362Q mutant channel in the presence of the resin-acid derivative Wu50. **I)** Scheme of putative interactions between Wu50 in the S4/pore site in the WT and the various mutants investigated. The putative effect of the resin acid derivative located in the S4/pore site (purple triangle) is shown by a purple arrow. The endogenous gating charge arginines (R362 (=R1), R365 (=R2)) are denoted by filled blue circles, F416 by a filled grey circle and W454 by a filled yellow circle. Mutations are denoted by empty black circles. **J)** Wu50-induced changes in G_{MAX} for different Shaker K_V-channel mutants. 100 µM, pH = 9. Mean ± SEM (n = 3–6). The effect is compared with a value of 1. *, p < 0.05; **, p < 0.01; ***, p < 0.001; ****, p < 0.0001

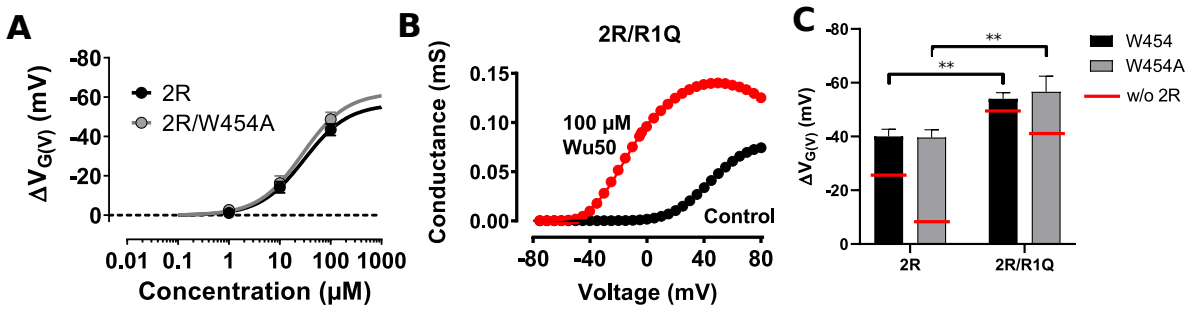

FIGURE 4. The 2R motif overrides the effect from the S4/pore site. A) Concentration-response curves for Wu50 at pH 9.0. 2R motif: EC_{50} = 30.0 ± 5.0 µM, ΔV_{MAX} = –56.5 ± 2.6 mV, n = 4-10; 2R motif/W454A: EC_{50} = 27.9 ± 9.2 µM, ΔV_{MAX} = –62.3 ± 6.5 mV, n = 3. Mean ± SEM. **B)** 100 µM Wu50 at pH 9.0 shifts $G(V)$ for the 2R motif/R362Q Shaker Kv channel results by –59.0 mV. **C)** Wu50-induced $G(V)$ shifts for Shaker K_V channel mutants as indicated. 100 µM, pH = 9. Mean ± SEM (n = 4-10).). **, p < 0.01. The red lines denote the shifts in the absence of the double arginine mutation (M356R/A359R = 2R).

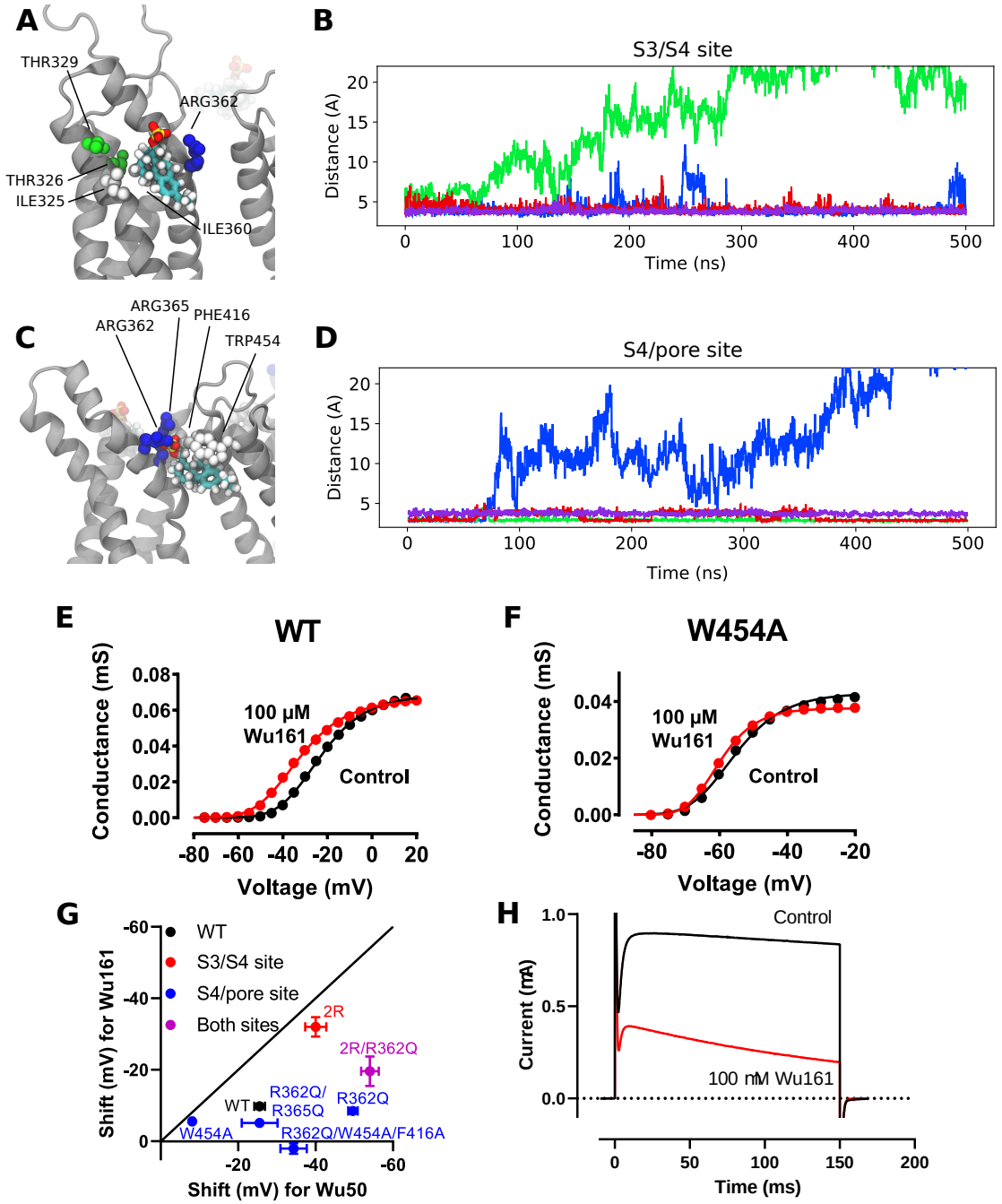

FIGURE 5. Wu161 binding to the S3/S4 and the S4/pore sites A) Zoomed-in side view of the S3/S4 site in the presence of wu161. **B)** Distance between closest atoms of Wu161 and I360 along a 500 ns long MD simulation of the WT channel system. Each of four subunits is depicted in a different color. **C)** Zoomed-in side view of the S4/pore site in the presence of Wu161. In A and C the channel is shown as grey ribbons, the Wu161 compounds are displayed as sticks, each atom type colored differently (yellow: S; cyan: C; red: O; blue: N and white: H) Apolar, polar, positively and negatively charged and Trp residues are represented as space-filling and depicted in white, green, blue, red and yellow, respectively. **D)** Distance between closest atoms of Wu161 and R362 along a 500 ns long MD simulation

of the WT channel system. Each of four subunits is depicted in a different color. **E-F)** $G(V)$ curves before and after application of 100 µM Wu161 to the channels as denoted. $G(V)$ shifts = –10.4 mV and –4.7 mV respectively. pH = 7.4. **G)** Correlation between $G(V)$ shifts for Wu50 and Wu161 (100 µM) on different Shaker mutants. Error bars represent Mean ± SEM (n = 4). The continuous line has a slope of 1. **H)** Wu161 speeds up inactivation of R362Q/F416A/W454A.

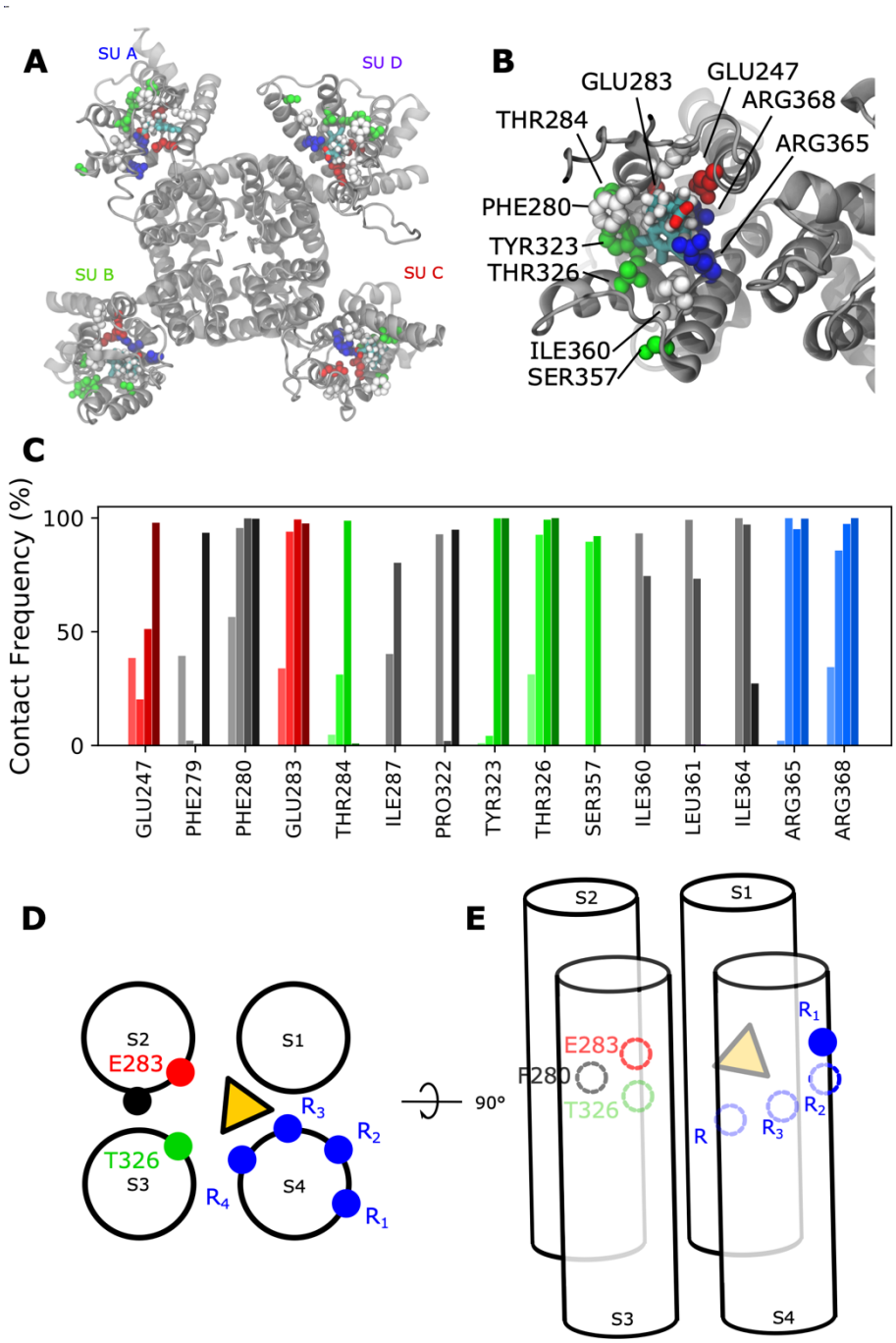

FIGURE 6 A possible binding site at the extracellular side of the VSD A) Top view of a representative snapshot of the interaction between Wu50 and the top-VSD site in the WT channel. The channel is shown as grey ribbons, the Wu50 compounds are displayed as sticks,

each atom type colored differently (cyan: C or Cl; red: O; blue: N and white: H) Apolar, polar, positively and negatively charged residues are represented as space-filling and depicted in white, green, blue and red, respectively. **B)** Zoomed-in top view of the top-VSD binding site for the WT channel in the presence of resin acid derivative Wu50. **C)** Contact frequency between any atom of Wu50 and the top-VSD site residues in the WT channel simulation. Apolar, polar, positively and negatively charged residues are depicted in shades of grey, green, blue and red, respectively. For each residue, each bar corresponds to the contact frequency for one of the four subunits. **D)** Top and **E)** side schematic view of the putative effect of resin acid derivative binding to the top-VSD site (yellow triangle) The endogenous gating charge arginines (R362, R365, R368 and R372) are denoted by blue filled circles. The positions of F280, E283, and T326 are denoted by black, red and green circles, respectively.

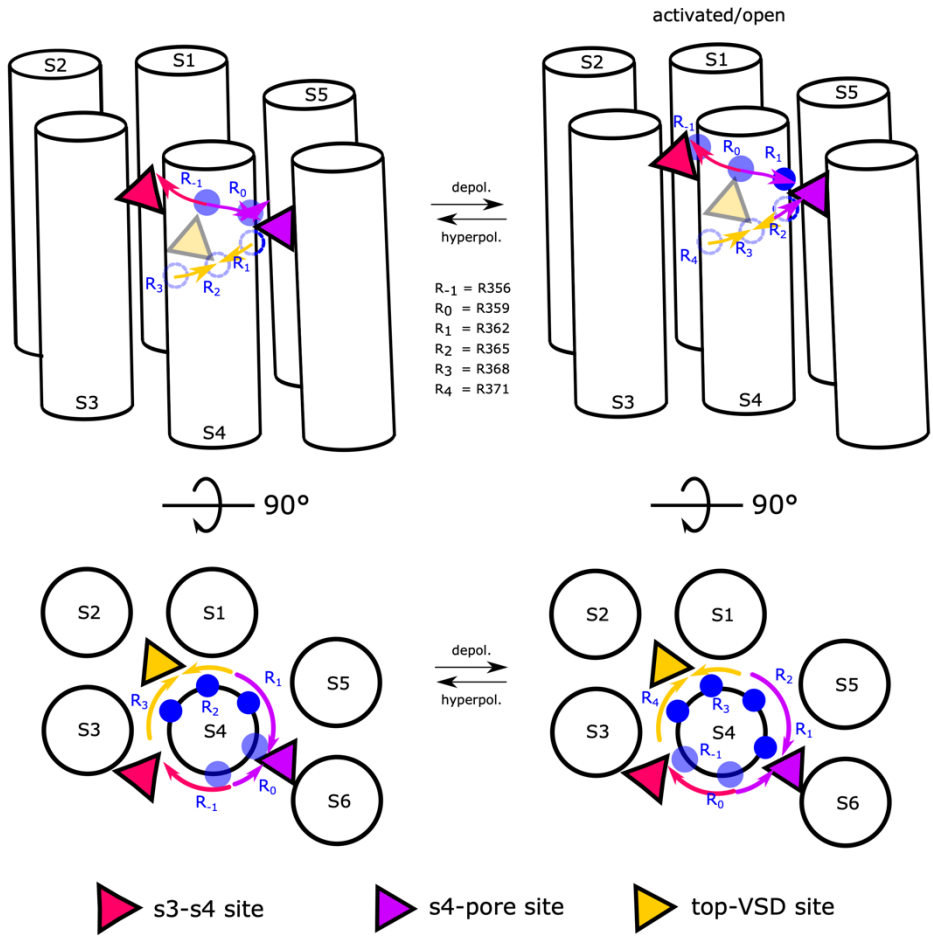

FIGURE 7 Three putative resin-acid binding sites act on activation via regulating S4 helical-screw motion. Side and top views of the motion of S4 during the last step of activation occurring in one subunit (N.B. the pore domain and VSD are from two different subunits). The S3/S4 site is represented as a red triangle, the S4/pore site as a purple triangle and the top-VSD site as a yellow triangle. The endogenous charged residues are shown as dark blue filled circles (dashed circles when hidden by S4). The two additional charges of the 2R motif are displayed as light blue filled circles. In the last intermediate (closed) state, a

compound bound to the S3/S4 site drags M356R (R_{-1}) upwards and clockwise (when viewed from the extracellular solution); a compound bound to the S4/pore site drags M356R (R_{-1}) downwards and counter clockwise, maintains A359R (R_0) in place and drags R362 (R_1) and R365 (R_2) upwards and clockwise; a compound bound at the top-VSD site drags R368 (R_3) upwards and clockwise and R362 (R_1) and R365 (R_2) downwards and counter clockwise. In the fully activated (open) state, a compound bound to the S3/S4 site maintains M356R (R_{-1}) in place, drags A359R (R_0) upwards and clockwise; a compound bound to the S4/pore site drags A359R (R_0) downwards and counter clockwise, maintains R362 (R_1) in place and drags R365 (R_2) and R368 (R_3) upwards and clockwise; a compound bound to the top-VSD site drags R362 (R_1) and R365 (R_2) downwards and counter clockwise, maintains R368 (R_3) in place, and drags R371 (R_4) upwards and clockwise.

SUPPLEMENTARY FIGURES

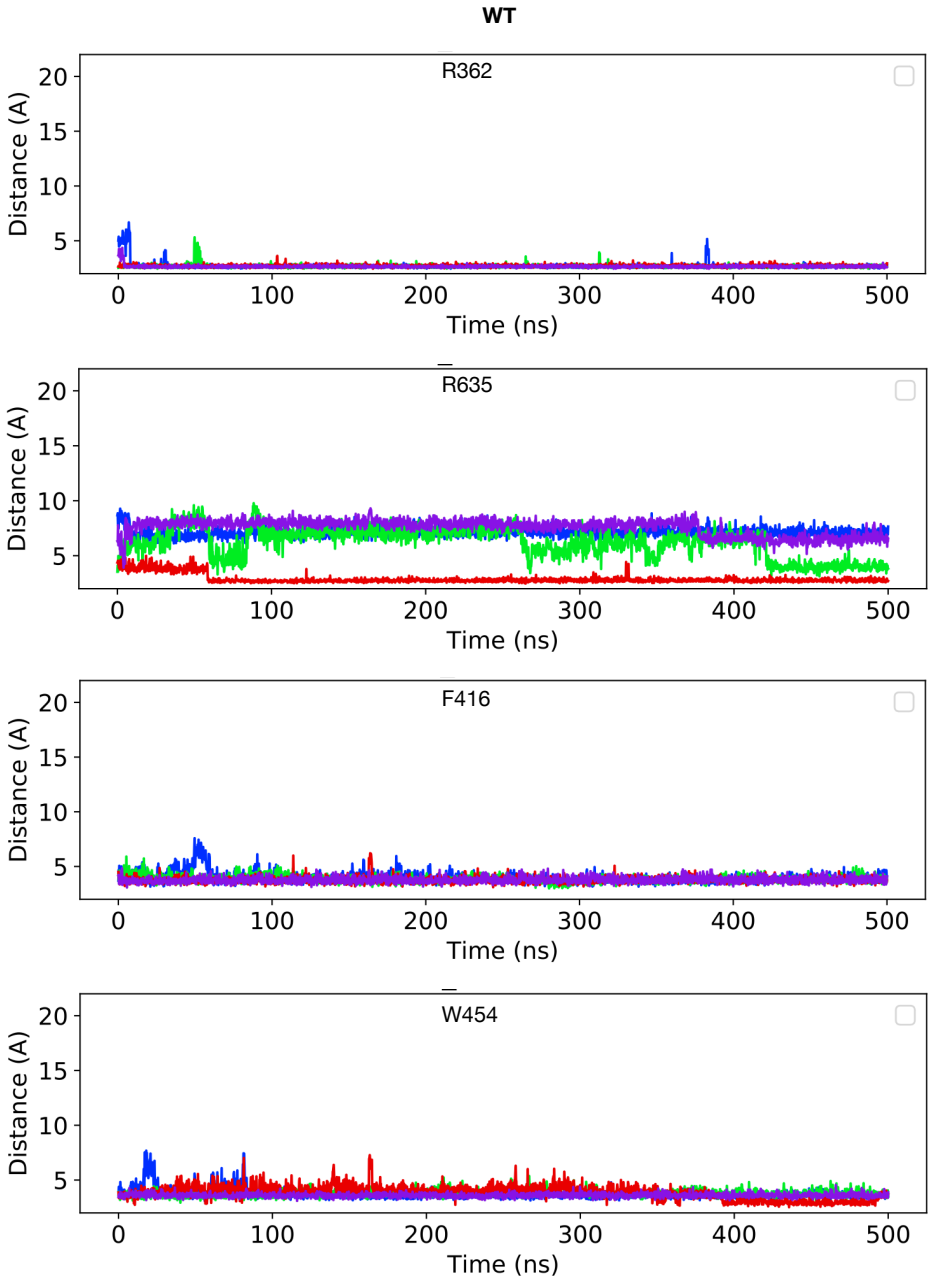

Figure S1 Distance between closest atoms of Wu50 and R362, R365, F416 and W454 along the MD simulations of the WT channel system. Each of four subunits is depicted in a different color.

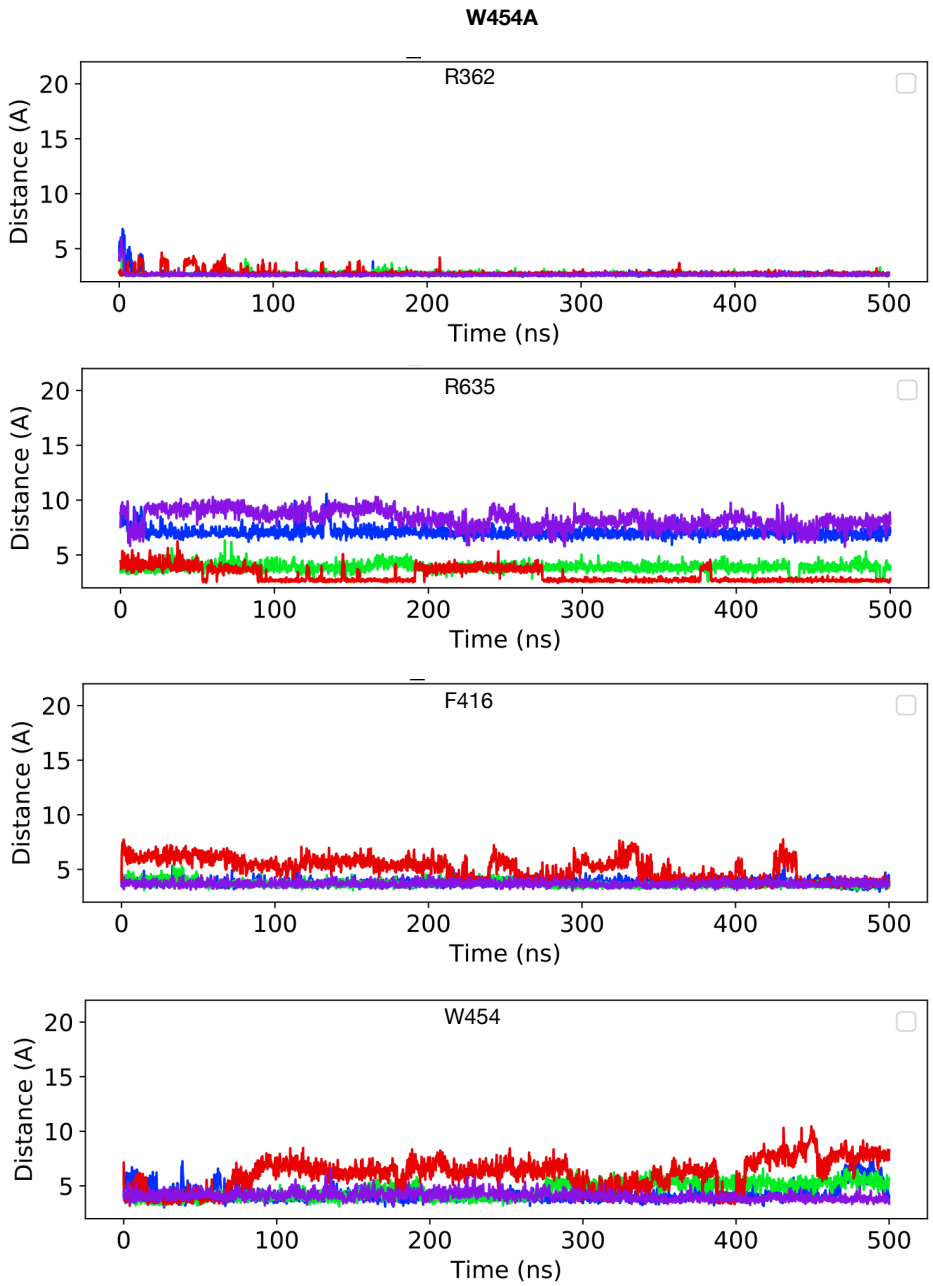

Figure S2 Distance between closest atoms of Wu50 and R362, R365, F416 and W454 along the MD simulations of the W454A channel system. Each of four subunits is depicted in a different color.

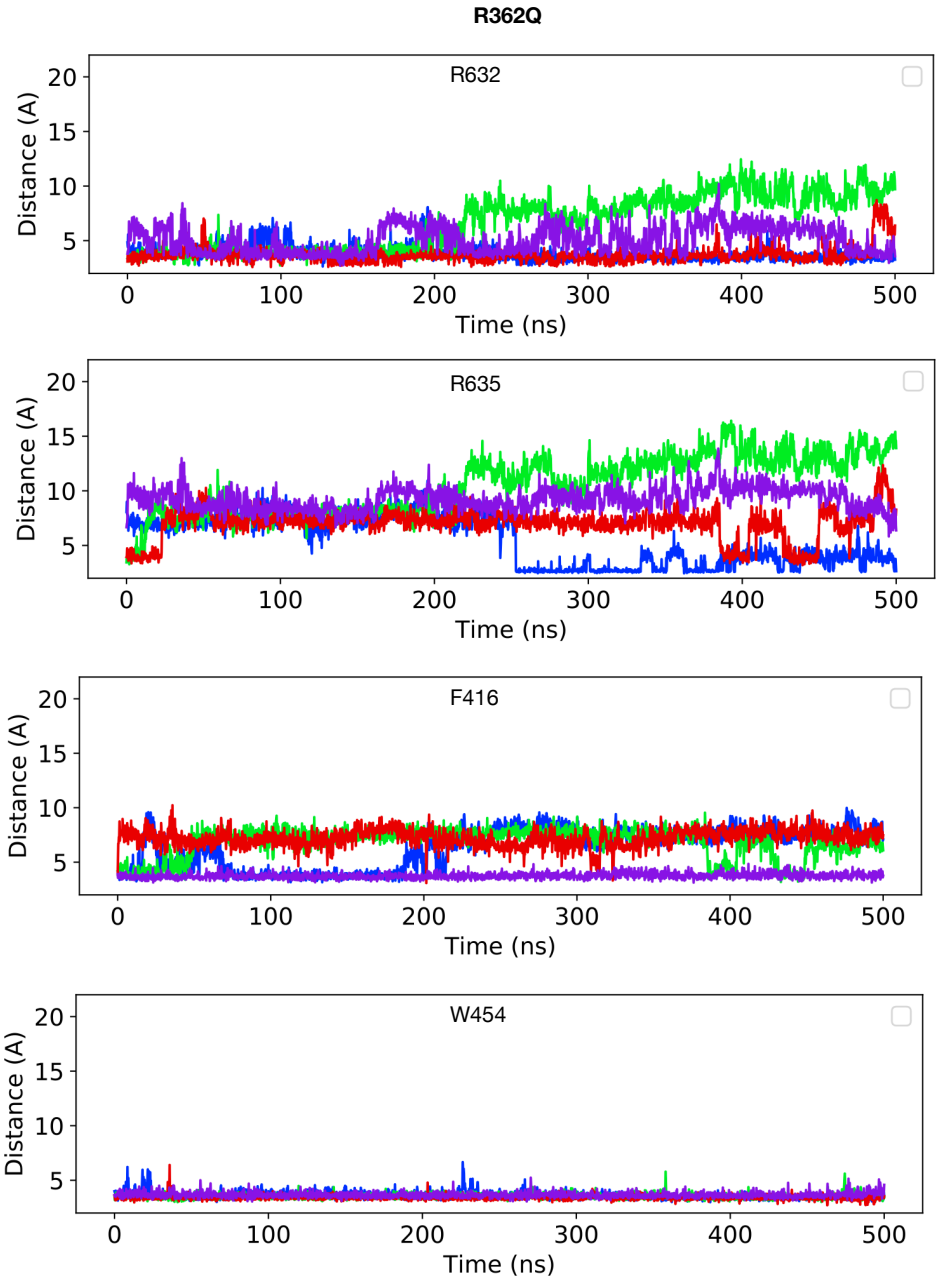

Figure S3 Distance between closest atoms of Wu50 and R362, R365, F416 and W454 along the MD simulations of the R362Q channel system. Each of four subunits is depicted in a different color.

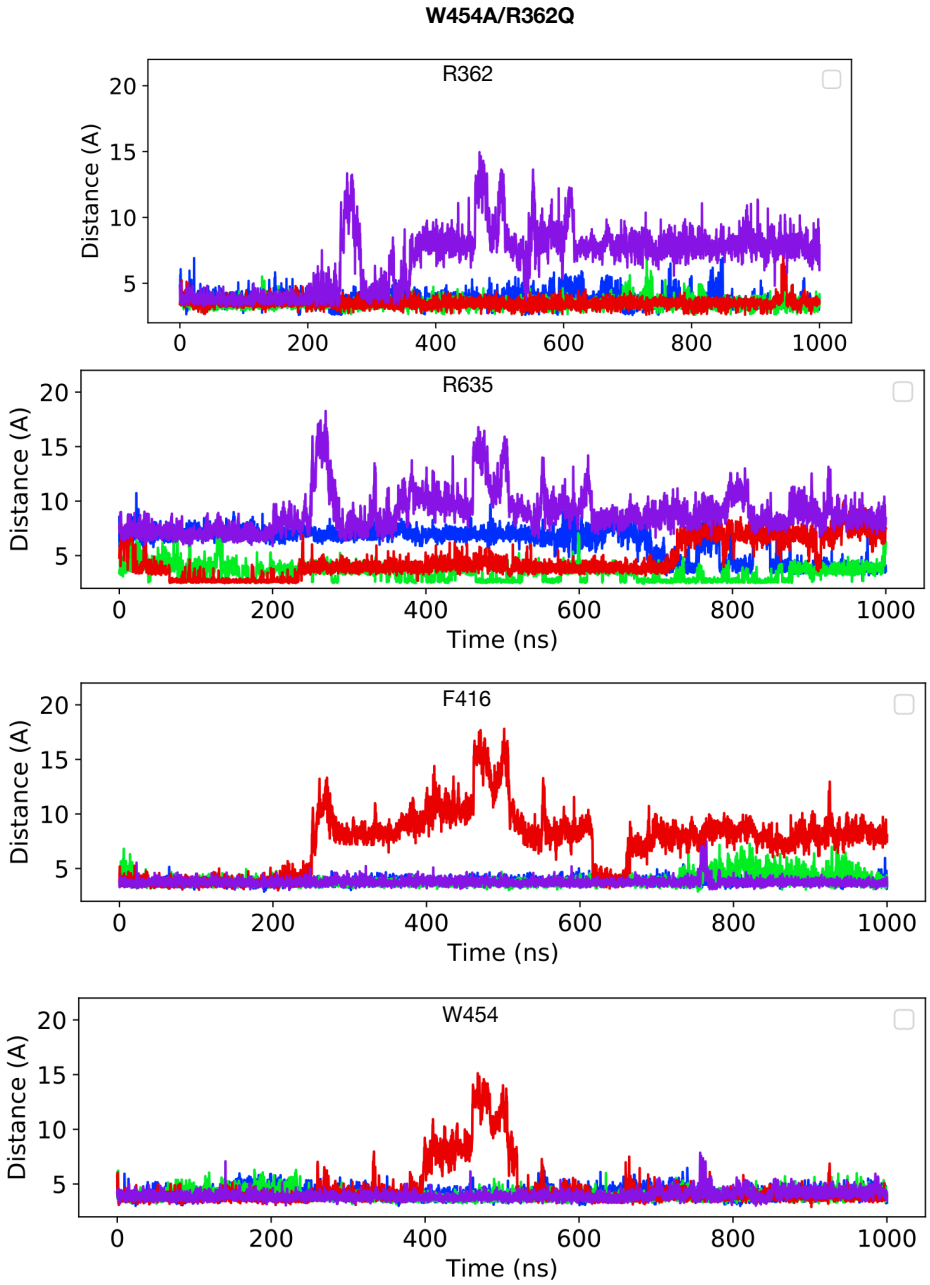

Figure S4 Distance between closest atoms of Wu50 and R362, R365, F416 and W454 along the MD simulations of the W454A/R362Q channel system. Each of four subunits is depicted in a different color.

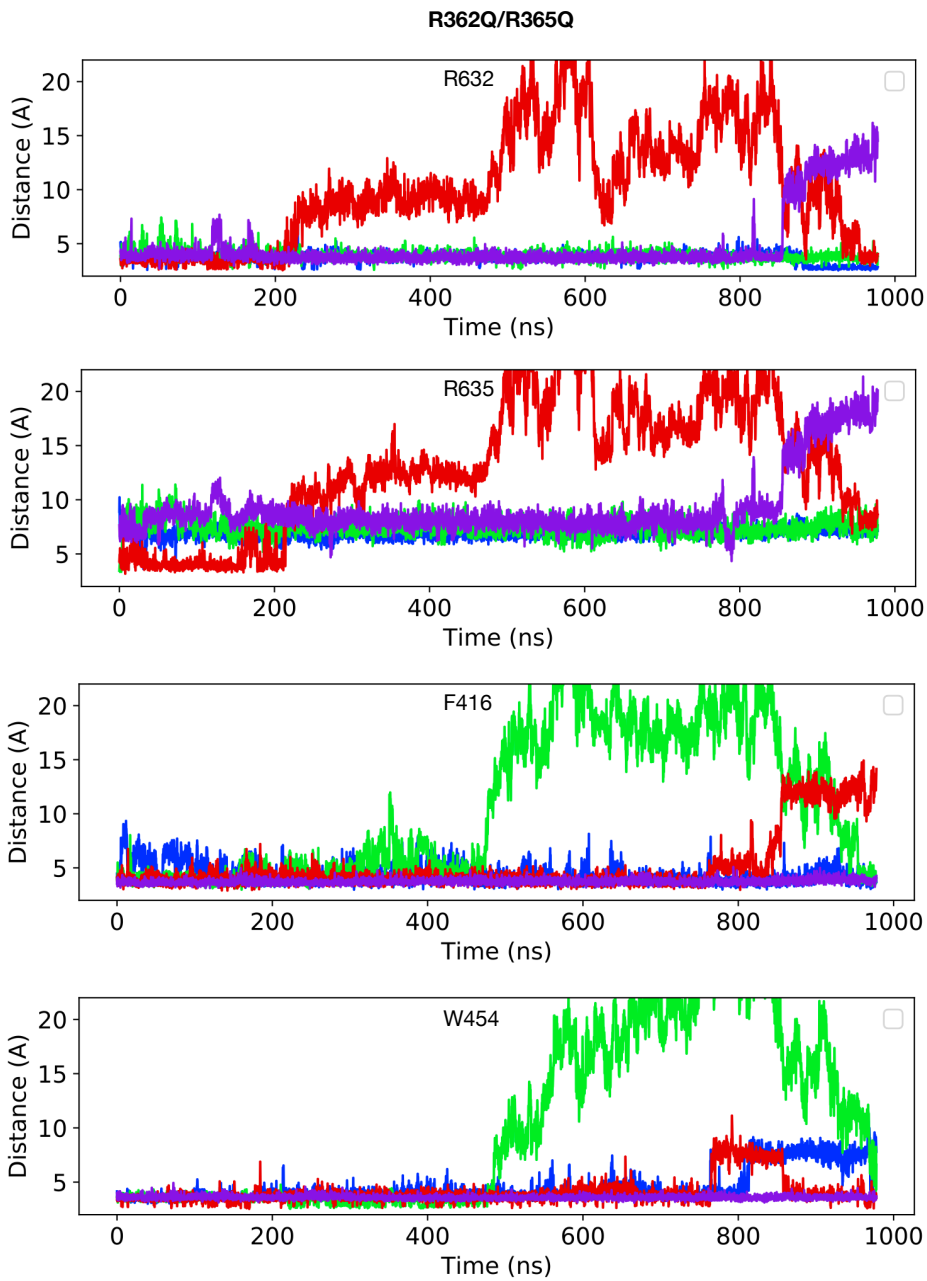

Figure S5 Distance between closest atoms of Wu50 and R362, R365, F416 and W454 along the MD simulations of the R362Q/R365Q channel system. Each of four subunits is depicted in a different color.

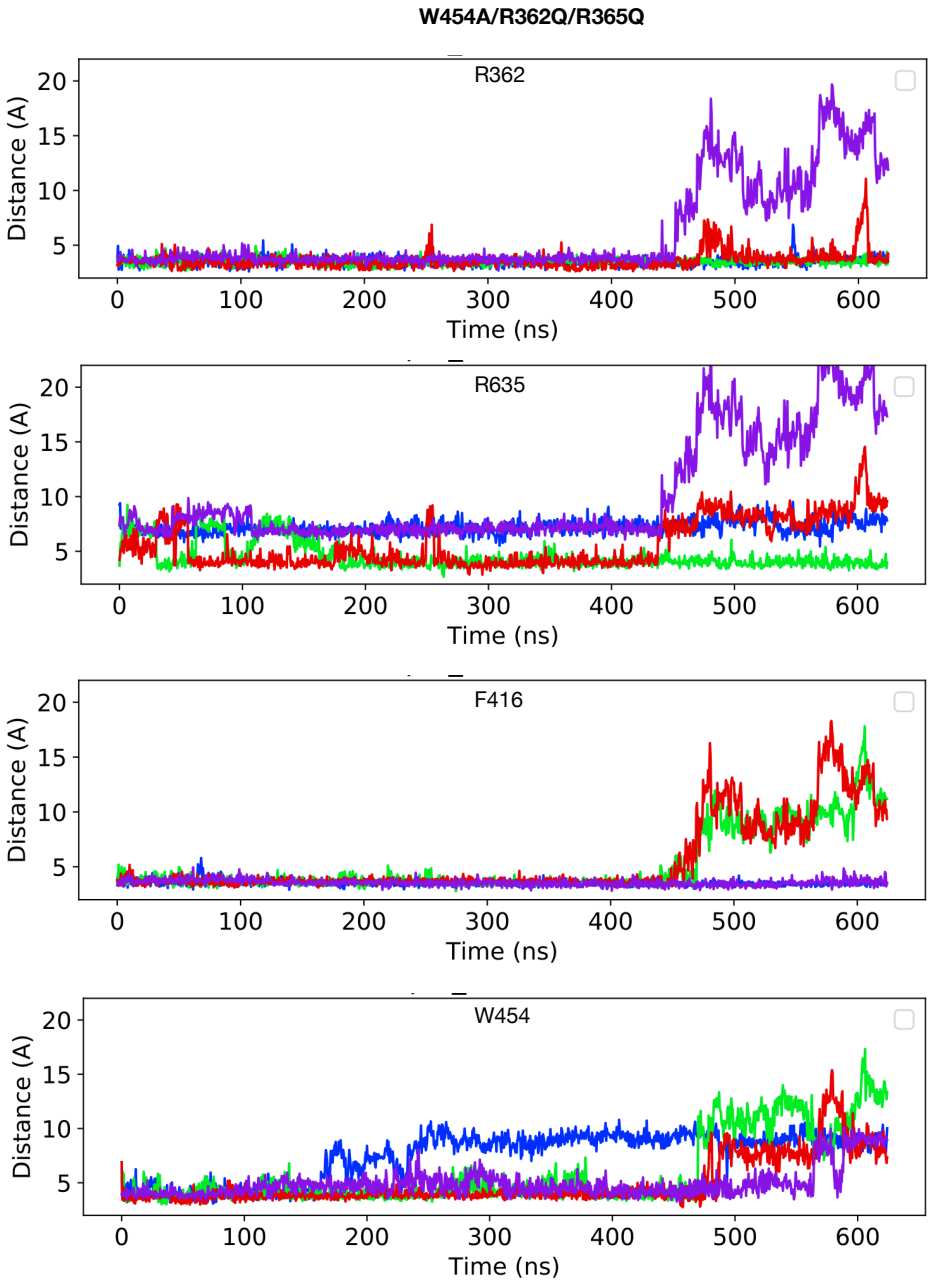

Figure S6 Distance between closest atoms of Wu50 and R362, R365, F416 and W454 along the MD simulations of the R362Q/R365Q/W454A channel system. Each of four subunits is depicted in a different color.

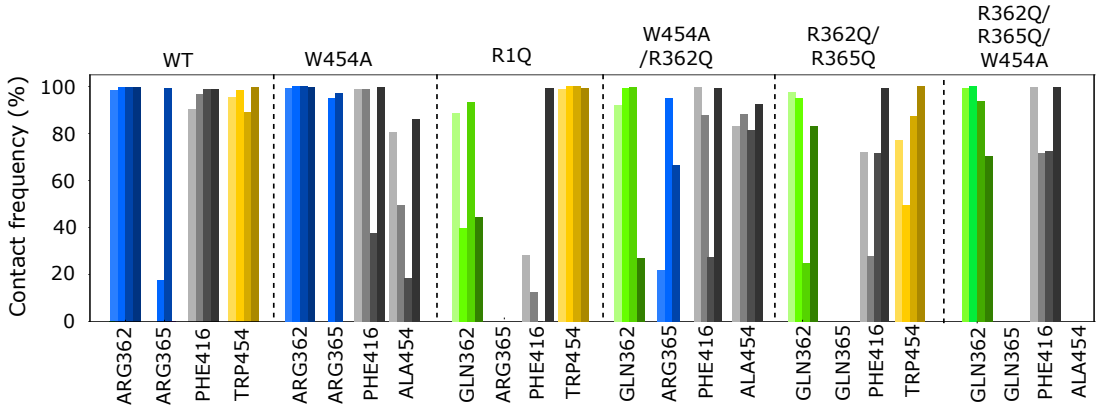

Figure S7 Contact frequency between any atom of Wu50 and select S4/pore site residues in the WT, W454A, R362Q, W454A/R362Q, R362Q/R365Q, W454A/R362Q/R365Q channel simulations. Apolar, positively charged and Trp residues are depicted in shades of grey, blue and yellow, respectively. For each residue, each bar corresponds to the contact frequency for one of the four subunits.

```
           e.c.      S4       i.c.   i.c.        S5        e.c.        e.c.              S6                i.c.

         356359362365                                 416          454
          ↓  ↓  ↓  ↓                                   ↓            ↓
Shaker   MSLAILRVIRLVRVFRIFKLSRH   RELGLLIFFLFIGVVLFSSAVYFAEA   PVGVWGKIVGSLCAIAGVLTIALPVPVIVSNFNYFYHRET
hKv1.1   TSLAILRVIRLVRVFRIFKLSRH   RELGLLIFFLFIGVILFSSAVYFAEA   PVTIGGKIVGSLCAIAGVLTIALPVPVIVSNFNYFYHRET
hKv1.2   MSLAILRVIRLVRVFRIFKLSRH   RELGLLIFFLFIGVILFSSAVYFAEA   PTTIGGKIVGSLCAIAGVLTIALPVPVIVSNFNYFYHRET
hKv1.3   MSLAILRVIRLVRVFRIFKLSRH   RELGLLIFFLFIGVILFSSAVYFAEA   PVTIGGKIVGSLCAIAGVLTIALPVPVIVSNFNYFYHRET
hKv1.4   MSFAILRIIRLVRVFRIFKLSRH   RELGLLIFFLFIGVILFSSAVYFAEA   PITVGGKIVGSLCAIAGVLTIALPVPVIVSNFNYFYHRET
hKv1.5   MSLAILRVIRLVRVFRIFKLSRH   RELGLLIFFLFIGVILFSSAVYFAEA   PITVGGKIVGSLCAIAGVLTIALPVPVIVSNFNYFYHRET
hKv1.6   MSLAILRVIRLVRVFRIFKLSRH   RELGLLIFFLFIGVILFSSAVYFAEA   PMTVGGKIVGSLCAIAGVLTIALPVPVIVSNFNYFYHRET
hKv1.7   MSLAILRVIRLVRVFRIFKLSRH   RELGLLIFFLFIGVVLFSSAVYFAEV   PVTVGGKIVGSLCAIAGVLTISLPVPVIVSNFSYFYHRET
hKv1.8   MSLAILRIIRLVRVFRIFKLSRH   RELGLLIFFLFIGVILFSSAVYFAEV   PTTPGGKIVGTLCAIAGVLTIALPVPVIVSNFNYFYHRET

hKv2.1   NVRRVVQIFRIMRILRILKLARH   NELGLLILFLAMGIMIFSSLVFFAEK   PKTLLGKIVGGLCCIAGVLVIALPIPIIVNNFSEFYKEQK
hKv2.2   NVRRVVQIFRIMRILRILKLARH   NELGLLILFLAMGIMIFSSLVFFAEK   PKTLLGKIVGGLCCIAGVLVIALPIPIIVNNFSEFYKEQK

hKv3.1   DVLGFLRVVRFVRILRIFKLTRH   NEFLLLIIFLALGVLIFATMIYYAER   PQTWSGMLVGALCALAGVLTIAMPVPVIVNNFGMYYSLAM
hKv3.2   DVLGFLRVVRFVRILRIFKLTRH   NEFLLLIIFLALGVLIFATMIYYAER   PQTWSGMLVGALCALAGVLTIAMPVPVIVNNFGMYYSLAM
hKv3.3   DVLGFLRVVRFVRILRIFKLTRH   NEFLLLIIFLALGVLIFATMIYYAER   PKTWSGMLVGALCALAGVLTIAMPVPVIVNNFGMYYSLAM
hKv3.4   DVLGFLRVVRFVRILRIFKLTRH   NEFLLLIIFLALGVLIFATMIYYAER   PKTWSGMLVGALCALAGVLTIAMPVPVIVNNFGMYYSLAM

hKv4.1   DVSGAFVTLRVFRVFRIFKFSRH   SELGFLLFSLTMAIIIFATVMFYAEK   PSTIAGKIFGSICSLSGVLVIALPVPVIVSNFSRIYHQNQ
hKv4.2   DVSGAFVTLRVFRVFRIFKFSRH   SELGFLLFSLTMAIIIFATVMFYAEK   PKTIAGKIFGSICSLSGVLVIALPVPVIVSNFSRIYHQNQ
hKv4.3   DVSGAFVTLRVFRVFRIFKFSRH   SELGFLLFSLTMAIIIFATVMFYAEK   PKTIAGKIFGSICSLSGVLVIALPVPVIVSNFSRIYHQNQ

hKv7.1   FATSAIRGIRFLQILRMLHVDRQ   QELITTLYIGFLGLIFSSYFVYLAEK   PQTWVGKTIASCFSVFAISFFALPAGILGSGFALKVQQKQ
hKv7.2   FATSALRSLRFLQILRMIRMDRR   KELVTAWYIGFLCLILASFLVYLAEK   PQTWNGRLLAATFTLIGVSFFALPAGILGSGFALKVQEQH
hKv7.3   LATS LRSLRFLQILRMLRMDRR   KELITAWYIGFLTLILSSFLVYLVEK   PKTWEGRLIAATFSLIGVSFFALPAGILGSGLALKVQEQH
hKv7.4   FATSALRSMRFLQILRMVRMDRR   KELITAWYIGFLVLIFASFLVYLAEK   PHTWLGRVLAAGFALLGISFFALPAGILGSGFALKVQEQH
hKv7.5   FATSALRSLRFLQILRMVRMDRR   KELITAWYIGFLVLIFSSFLVYLVEK   PLTWLGRLLSAGFALLGISFFALPAGILGSGFALKVQEQH
```

Figure S8 Sequence alignment between segments S4, S5 and S6 in several K_V channel families, highlighting positively and negatively charged residues (blue and red, respectively) as well as aromatic ones (green). Gray bars are approximate transmembrane helical segments. E.c. = extracellular. i.c. = intracellular. Arrows denote mutated residues in the present investigation.

SUPPLEMENTARY TABLES

Table S1: Summary of G/V shifts and Gmax for the mutants reported in this paper

	Wu50 (pH 9.0)						Wu161 (pH 7.4					
Mutant	**ΔVG(V) (mV)**			**Gmax (rel.)**			**ΔVG(V) (mV)**			**Gmax (rel.)**		
	Mean	SEM	n	**Mean**	SEM	n	Mean	SEM	n	**Mean**	SEM	n
M356R/A359R (=3R)	-40.0	2.7	10	1.58	0.09	8	-32.0	2.7	6	1.20	0.05	6
M356R/A359R/W454A	-39.6	2.9	5	1.28	0.09	5						
M356R/A359R/R362Q	-54.0	2.3	4	1.93	0.25	4	-19.6	4.1	5	1.19	0.07	5
M356R/A359R/R362Q/W454A	-56.6	5.8	4	1.50	0.14	4						
WT	-25.5	1.4	5	1.36	0.07	6	-9.8	1.1	5	1.03	0.04	3
W454A	-8.1	0.4	5	0.56	0.08	5	-5.6	0.8	4	0.86	0.04	4
R362Q	-49.6	1.2	3	1.25	0.14	3	-8.5	0.5	3	1.05	0.01	4
R362Q/W454A	-41.0	4.4	5	1.28	0.08	5						
R362Q/W454A/F416A	-34.3	3.4	3	0.17	0.06	5	2.0	1.4	4	0.47	0.07	4
R362Q/R365Q	-25.5	4.6	5	0.55	0.12	5	-5.2	1.2	4	0.99	0.03	4
R362Q/R365Q/W454A	-24.7	3.0	5	0.57	0.13	6						
R362Q/R365Q/W454A/F280I	ND	N/A	N/A	0.05	0.02	4	1.1	3.1	3	0.64	0.12	3